frontiers | Frontiers in Soft Matter

TYPE Original Research
PUBLISHED 27 March 2024
DOI 10.3389/frsfm.2024.1341129

Check for updates

OPEN ACCESS

EDITED BY
Frank Alexis,
Universidad San Francisco de Quito, Ecuador

REVIEWED BY
Luca Lanotte,
INRA Centre Bretagne-Normandie, France
Alejandro D. Rey,
McGill University, Canada
Matthew Harrington,
McGill University, Canada

*CORRESPONDENCE
Konstantin G. Kornev,
kkornev@clemson.edu

†These authors have contributed equally to this work

RECEIVED 19 November 2023
ACCEPTED 13 February 2024
PUBLISHED 27 March 2024

CITATION
Aprelev P, Brasovs A, Bruce TF, Beard CE, Adler PH and Kornev KG (2024), To seal a wound, caterpillars transform blood from a viscous to a viscoelastic fluid in a few seconds. *Front. Soft Matter* 4:1341129. doi: 10.3389/frsfm.2024.1341129

COPYRIGHT
© 2024 Aprelev, Brasovs, Bruce, Beard, Adler and Kornev. This is an open-access article distributed under the terms of the Creative Commons Attribution License (CC BY). The use, distribution or reproduction in other forums is permitted, provided the original author(s) and the copyright owner(s) are credited and that the original publication in this journal is cited, in accordance with accepted academic practice. No use, distribution or reproduction is permitted which does not comply with these terms.

# To seal a wound, caterpillars transform blood from a viscous to a viscoelastic fluid in a few seconds

Pavel Aprelev[1†], Artis Brasovs[1†], Terri F. Bruce[2], Charles E. Beard[3], Peter H. Adler[3] and Konstantin G. Kornev[1*]

[1]Department of Materials Science and Engineering, Clemson University, Clemson, SC, United States, [2]Light Imaging Facility, Clemson University, Clemson, SC, United States, [3]Department of Plant and Environmental Sciences, Clemson University, Clemson, SC, United States

In insects vulnerable to dehydration, the mechanistic reaction of blood after wounding is rapid. It allows insects to minimize blood loss by sealing the wound and forming primary clots that provide scaffolding for the formation of new tissue. Using nano-rheological magnetic rotational spectroscopy with nickel nanorods and extensional rheology, we studied the properties of blood dripping from the wound of caterpillars of the Carolina sphinx moth (*Manduca sexta*) with a high concentration of blood cells. We discovered that wound sealing followed a two-step scenario. First, in a few seconds, the Newtonian low-viscosity blood turns into a non-Newtonian viscoelastic fluid that minimizes blood loss by retracting the dripping blood back into the wound. Next, blood cells aggregate, starting from the interfaces and propagating inward. We studied these processes using optical phase-contrast and polarized microscopy, X-ray imaging, and modeling. Comparative analyses of the cell-rich and cell-poor blood of different insects revealed common features of blood behavior. These discoveries can help design fast-working thickeners for vertebrate blood, including human blood.

KEYWORDS

**cell aggregation, hemolymph, hemocytes, clotting kinetics, Lepidoptera, rheology**

## 1 Introduction

Insects have developed special strategies to deal with wounding and potential infection (Salt, 1970; Wigglesworth and Gupta, 1979; Gillespie et al., 1997; Theopold et al., 2002; Strand, 2008; Dushay, 2009; Jiang et al., 2010; Hillyer and Strand, 2014; Eleftherianos et al., 2021). Wounding triggers humoral and cellular reactions associated with insect blood (hemolymph) (Salt, 1970; Gregoire and Rockstein, 1974; Wigglesworth and Gupta, 1979; Bohn and Brehelin, 1986; Gillespie et al., 1997; Theopold et al., 2002; Strand, 2008; Dushay, 2009; Jiang et al., 2010; Hillyer and Strand, 2014; Eleftherianos et al., 2021). These reactions span spatial scales, from the nanometer to microscopic level, and time scales, from microseconds to hours. At the wound site, a primary clot nucleates within minutes after wounding (Salt, 1970; Wigglesworth and Gupta, 1979), while the formation of a scab and new epidermal tissue happen on a time scale more than two orders of magnitude greater (Salt, 1970; Wigglesworth and Gupta, 1979; Parle et al., 2016). The physical features of primary clot formation in the first minutes of hemolymph leakage from the wound are

not sufficiently detailed, and a quantitative analysis of the kinetics of clot nucleation in cell-rich hemolymph was only recently reported (Aprelev et al., 2019).

The concentration of cells (hemocytes) in the blood of different insect species varies significantly; hence, insects developed various strategies for wound sealing. In the hemocyte-poor hemolymph, as in butterflies and moths, the humoral reactions in the plasma cause the self-assembly of lipoproteins (Bohn and Brehelin, 1986; Zdybicka-Barabas and Cytrynska, 2013; Ling et al., 2018; Miserez et al., 2023). Lipoproteins, with their surfactant-like action, recognize the foreign interface and immediately engage hemocytes or other large proteins, such as hemocytin (molecular weights of hemocytin in the moth *Bombyx mori* and the fly *Drosophila melanogaster* are ~260 and ~300 kDa, respectively) (Hu et al., 2024), to aggregate into filamentary threads consisting of more complex biopolymer subunits (Mulnix et al., 1995) and then into gel-like wound covers (Gregoire and Rockstein, 1974; Bohn and Brehelin, 1986). The gel tightening of the hemocytes at the wound surface renders the complex mesh impermeable to microorganisms and hinders water evaporation.

Lipoproteins are also found in the primary clots of the hemocyte-rich hemolymph (Brehelin, 1979; Boman and Hultmark, 1987; Chino et al., 1987; Mulnix et al., 1995; Theopold et al., 2004; Dushay, 2009; Jiang et al., 2010; Maravilla et al., 2020), such as exchangeable apolipophorin-III in the cockroach *Periplaneta americana* (Coodin and Caveney, 1992; Dushay, 2009). In contrast to the hemocyte-poor blood of butterflies and moths (Lepidoptera), the hemolymph of their larvae (i.e., caterpillars) is hemocyte-rich. The comparative biomolecular studies of clotting in lepidopteran larvae and adults and in other insects suggest that the hemocytin and lipoproteins common in adults and larvae could be among the first to respond and trigger complex immune reactions, resulting in the formation of filamentary structures and primary clots (Boman and Hultmark, 1987; Mulnix et al., 1995; Theopold et al., 2004; Rahman et al., 2006; Jiang et al., 2010; Zdybicka-Barabas and Cytrynska, 2013; Staczek et al., 2018; Maravilla et al., 2020; Hu et al., 2024).

The limiting step for primary clot formation in the larvae of the Carolina sphinx moth (*Manduca sexta*) is the aggregation of hemolymph cells (hemocytes), assisted by pseudopodia, the thread-like extensions of hemocytes (Gregoire, 1955). In the larvae of *M. sexta*, the cells aggregate in approximately 3–5 min. Within a few minutes, the cells consolidate, and the aggregate stiffens, as manifested by a weak elastic reaction (Aprelev et al., 2019) approximately 4–5 min from the moment of aggregation. The primary clot remains soft relative to the repaired wound (Parle et al., 2016) not only in Lepidoptera, such as *M. sexta*, but also in other insects. In *Drosophila*, for example, primary clots are initially soft and can be pulled from the hemolymph using a metal needle (Bidla et al., 2005). The biomechanics of primary clot nucleation, consolidation, and stiffening remain poorly understood.

In view of these knowledge gaps, we investigated the material properties of clotting hemolymph to reveal the physical determinants that stop the bleeding. The hemocyte-rich blood of the fifth-instar (i.e., mature) larvae of *M. sexta* was chosen as our model system.

We first studied the time needed for the insect to react to wounding and to stop the loss of hemocyte-rich hemolymph. For the caterpillars of *M. sexta*, the time to change the rheological properties of the hemolymph is surprisingly short, i.e., only a few seconds. This fast reaction and the small volume of the available droplets present a challenge to the investigation of the material properties of the hemolymph. Therefore, we developed new approaches to study the rheological and surface properties of the droplets. The comparative analysis of the short-time clotting phenomena associated with the preliminary sealing of the insect wound revealed a general strategy for wound healing: first, the insect turns the Newtonian, almost inviscid hemolymph into a viscoelastic fluid. The acquired elasticity prevents the hemolymph from escaping from the wound. The fluid film or a drop covering the wound surface then forms a crust prepared from a gel-like biopolymer mesh (in hemocyte-poor hemolymph) or a composite hemocyte-polymer mesh (in hemocyte-rich hemolymph).

# 2 Results

## 2.1 The time to stop the bleeding from the wound

To evaluate the relevant time scale of the formation of a primary clot, we used a setup (Figure 1A) in which the wound was oriented downward and the hemolymph dripped on its own. Caterpillars of 9–10 g and 1–2 days before pre-pupation were used. Each caterpillar was constrained in a tube, and the hemolymph was extracted via a 1–2-mm incision in the third proleg.

This setup allowed us to probe the dripping hemolymph several seconds after making the incision. Filming the features of the drop and liquid bridge formation had a success rate of approximately 5%, because shortly after the incision, the caterpillar moved vigorously, causing difficulties in focusing the camera. Nonetheless, our naked-eye observations and filming confirmed that in the first several seconds after the incision, the detachment of the falling drop from the wound followed the scenario common for simple fluids, such as water (Eggers, 1997; Montanero and Ponce-Torres, 2020); the drop formed a liquid bridge connecting it with the wound (Figure 2A), and then, the bridge necked (Figures 2B, C) and broke, producing satellites (Figures 2D, E). This behavior suggested that in the first seconds, a mostly water-like, low-viscosity hemolymph dripped from the wound.

During the next 5–10 s (i.e., ~10–15 s after incision), drop detachment showed a different scenario (Figure 3). The necking stage, shown in Figures 2B, C, proceeded similarly (Figures 3A, B), but after that, instead of breaking up the bridge, as shown in Figure 2D, the hemolymph formed filaments of uniform radii (Figure 3C). Before the breakup, the straight filament formed a bulge in the middle (Figure 3D), and the bulge grew to form a second drop (Figures 3E, F). The droplets moved toward the menisci pulled by the connecting filaments. The filaments that formed 10–15 s after the incision broke up in ~20–40 ms (Figure 3G).

During the next 50–60 s (i.e., ~75 s after incision), drop detachment followed the scenario shown in Figure 3 (Supplementary Video S1). However, the lifetime of these late filaments increased significantly by approximately one order of magnitude to ~240 μs.

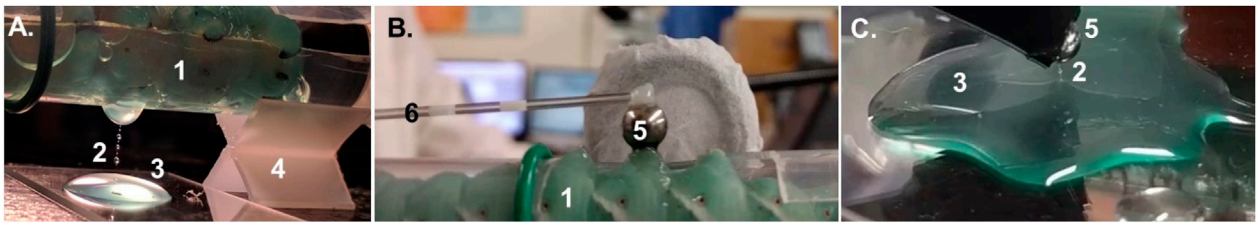


FIGURE 1
**(A)** Cylindrical plastic sleeve (1) supported by an X-shaped holder (4). The plastic sleeve has a window exposing a portion of the side of the mid-abdomen of a larva of *Manduca sexta* with a wounded proleg. The dripping hemolymph formed long filaments (2) with droplets. The hemolymph is collected in a Petri dish (3). **(B)** The sleeve (1) with the caterpillar is flipped upside down, and a metal ball (5) is brought in contact with the wound to form a hemolymph meniscus. The glass rod (6) with the ball (5) is controlled by a manipulator that allows the ball to be lifted to a prescribed height and to form a liquid bridge. **(C)** Hemolymph filament can be obtained from a pool of hemolymph, using either the same ball (5) as in **(B)** or by applying a rod (6).

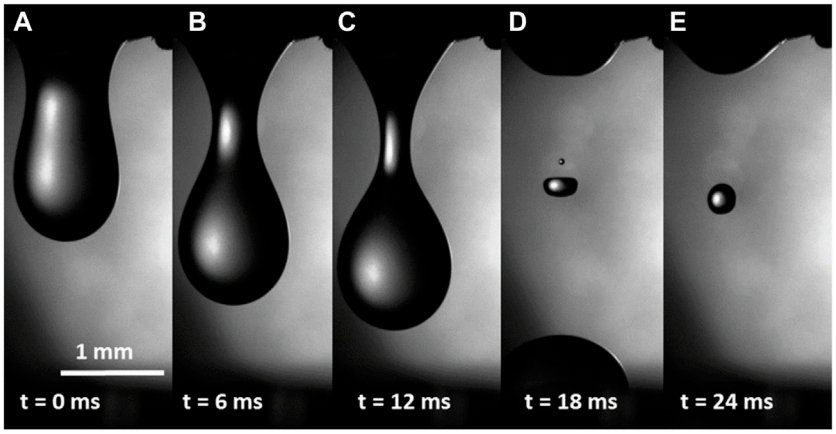


FIGURE 2
**(A–E)** Hemolymph dripping from the wound of a caterpillar several seconds after the wound was made. No filaments were observed, indicating that the hemolymph at this time scale was not highly viscous or elastic.

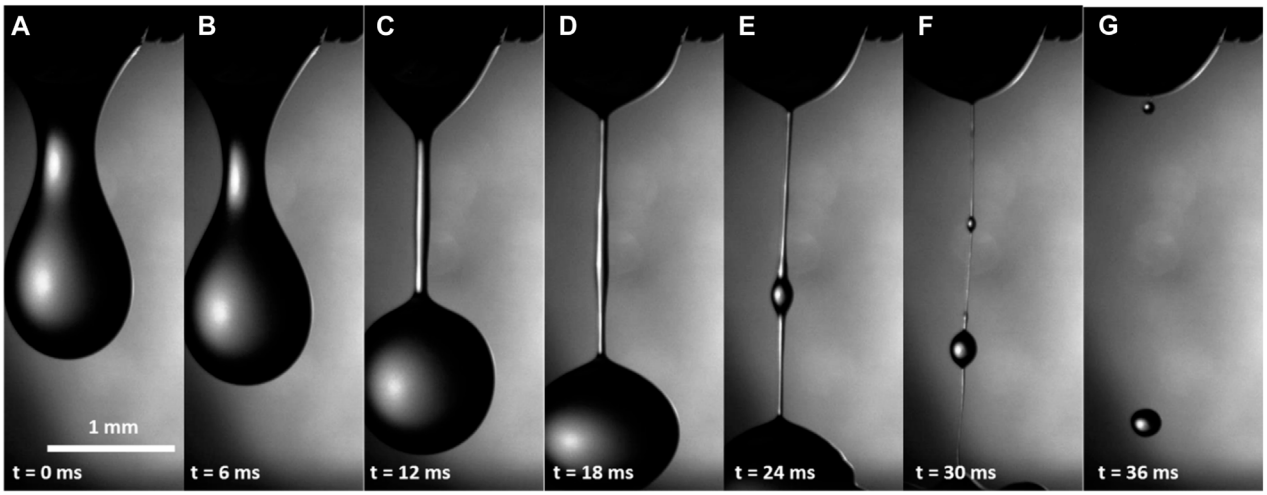


FIGURE 3
**(A–G)** Hemolymph dripping from the wound of a caterpillar within 10–15 s after wounding. A straight filament in **(D)** indicates that the hemolymph either increased its viscosity or became viscoelastic.

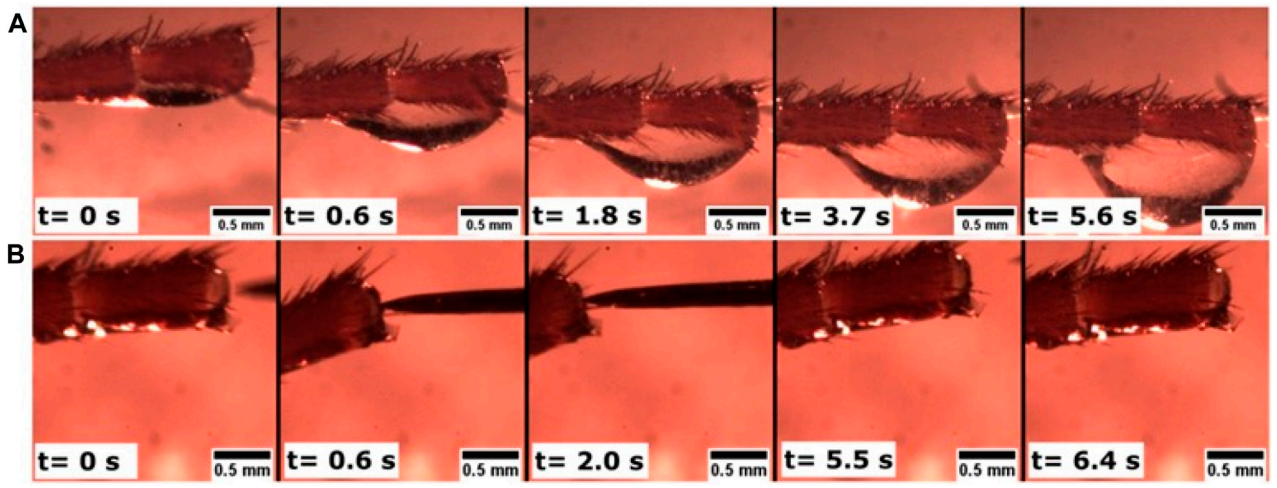


FIGURE 4
Hemolymph dripping from the severed antenna of the cockroach *Periplaneta americana*. The head (not pictured) is to the left. **(A)** After cutting off the end of the antenna, the hemolymph continued flowing to this end. Over approximately 6 s, a drop formed. After $t$ = 5.6 s, the drop fell, and no other drops appeared. **(B)** After ~10 min, the wound was completely sealed by a rigid crust: a tungsten needle was not able to penetrate the crust. When the needle was applied ($t$ = 0.6 s) to a cantilevered antenna, the antenna bent, tilting its end as shown in the figure. When the needle was removed ($t$ = 5.5 s and $t$ = 6.4 s), the antenna returned to its original state, and the sealed end appeared undeformed.

These results indicate that the properties of the hemolymph change quickly; the hemolymph starts dripping as an almost inviscid water-like fluid and then quickly changes its rheological properties. Typically, bleeding stopped after 60–90 s.

The scenario of wound sealing in the larvae of *M. sexta* was validated with that of the cockroach *P. americana* (Figure 4). Although the hemolymph composition of cockroaches could be somewhat different, both the insects have hemocyte-rich hemolymph (Chapman, 2013), and, as shown below, the plasma viscosity for both species is similar. After the detachment of an antennal flagellomere (i.e., an individual unit of the last antennal segment), a drop of hemolymph appeared at the cut end. The drop fell, and the remaining hemolymph moved back into the antennal lumen. No other drops appeared, and after approximately 10 min, the wound had sealed with a rigid crust.

The almost constant radius of the cylindrical filaments indicated that the hemolymph had either thickened by increasing its shear viscosity or had become elastic (McKinley and Sridhar, 2002; Montanero and Ponce-Torres, 2020). In other words, one could think of the filaments as being similar to those either produced by thick honey-like fluids or thin dog saliva-like fluids. To obtain honey-like filaments, the shear viscosity of the hemolymph must increase significantly. We, therefore, measured the shear viscosity by magnetic rotational spectroscopy (MRS) with nickel (Ni) nanorods.

## 2.2 Characterization of shear viscosity using magnetic rotational spectroscopy with nickel nanorods

Ferromagnetic nickel nanorods coated with poly(vinylpyrrolidone) were dispersed in a hemolymph drop and were continuously rotated by applying a rotating magnetic field and changing their rotating frequency $\omega_B$ (Gu and Kornev, 2016; Kornev et al., 2016; Aprelev et al., 2019; Brasovs et al., 2023). When an applied rotating magnetic field $\boldsymbol{B}$ acts on a nanorod of magnetization $M$ and volume $V$, it exerts a torque, $T_B = VMBsin(\omega_B t - \theta)$, forcing the nanorod to turn in the $B$-plane. The angle $\psi = \omega_B t - \theta$ specifies the angle that the magnetic moment forms with the magnetic field at time moment $t$. The magnetic moment is aligned with the nanorod axis, forming angle $\theta$ with a stationary reference axis (Figure 5).

When a nanorod rotates, it experiences resistance from the surrounding hemolymph. The MRS theory uses the Jeffery (Jeffery, 1922) model of rotation of an ellipsoid in a Newtonian fluid of viscosity $\eta$. Therefore, this technique provides the fluid viscosity at the zero shear rate. The torque on the nanorod of length $L_0$ and diameter $d$ is $T_\eta = \Gamma\eta d\theta/dt$, where $\Gamma = \frac{\pi {L_0}^3}{3ln(L_0/d)-2.4}$ is the nanorod form factor (Doi and Edwards, 1988). For nanorods, the inertial forces at the given frequencies are insignificant; thus, by balancing the mechanical and magnetic torques, $T_\eta = T_B$, we model and interpret the observed behavior and the rotational dynamics of the nanorods in different drops of the hemolymph.

The nanorods were tracked using a camera (Figures 5A–C), and the videos were post-processed to fit the nanorod angle versus time, using this model. Two distinguishable scenarios of nanorod rotation are shown in Figures 5D, E.

At low-driving frequencies, $\omega_B$, the nanorod rotated synchronously, lagging behind the field by a constant angle $\psi$. When the frequency $\omega_B$ increased above a certain critical value $\omega_c = VMB/(\Gamma\eta)$, the nanorod began to tumble (Figures 6A, B). By measuring $\omega_c$, as explained by Kornev et al. (1999); Gu and Kornev (2016); Aprelev et al. (2017); and Brasovs et al. (2023), we measured the shear viscosity of the hemolymph (Table 1). The hemolymph of all probed species showed Newtonian behavior. The shear viscosity of the probed hemolymph did not change over the first few minutes (Figures 6C, D). When probed using a cone-and-plate viscometer at a greater load, the *M. sexta* hemolymph showed Newtonian behavior as well (Kenny et al., 2018).

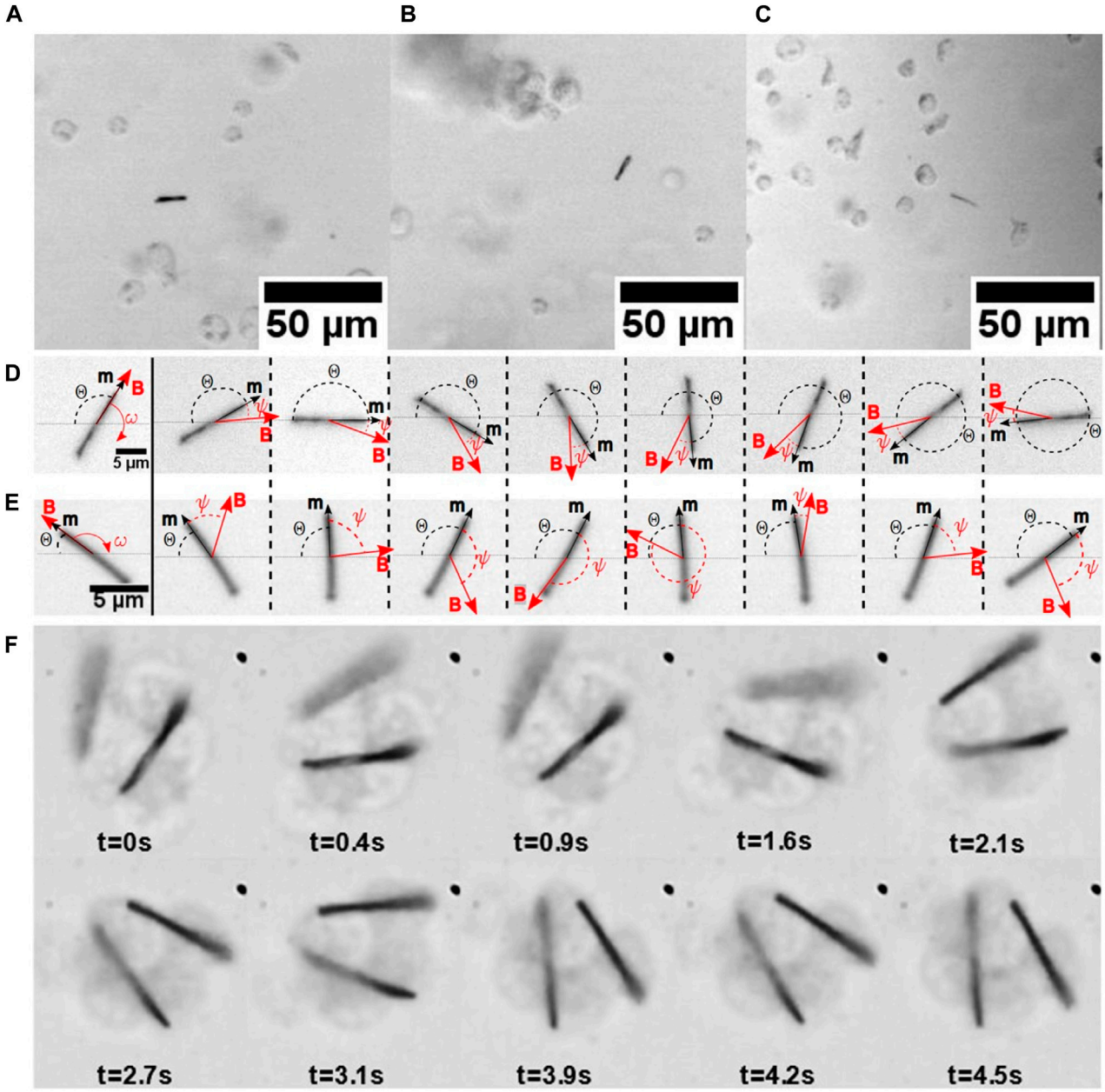


FIGURE 5
**(A)** Nickel nanorods in a hemolymph drop from the larvae of *M. sexta*. The different nanorods were imaged using a ×10 Olympus BX51 objective. The nanorods were observed through the hemolymph–air interface, and the images were taken at **(A)** $t$ = 5 *minutes*, **(B)** 11 *minutes*, and **(C)** 16 *minutes* after drop placement on the glass slide. **(D)** Synchronous rotation of a nanorod with the applied rotating field. The angle $\psi$ that the magnetic moment $\boldsymbol{m}$ forms with the field $\boldsymbol{B}$ is constant. **(E)** Asynchronous rotation of a nanorod with the applied rotating field. When the nanorod follows the applied magnetic field, it oscillates so that the angle $\psi$ periodically changes with time. **(F)** Hemocytes attach themselves to the nanorods. Applying a rotating magnetic field, the aggregate can rotate in an asynchronous regime.

This analysis of the shear viscosity suggests that the hemolymph dripping from the wound does not behave as a thick honey-like fluid. Furthermore, the hemocytes had no time to aggregate. Therefore, the appearance of cylindrical filaments when the hemolymph drips from the wound cannot be explained by the significant increase in its shear viscosity.

Thus, we hypothesized that as the first step in primary clot formation, the hemolymph has to be turned into a viscoelastic fluid.

## 2.3 Extensional rheology of hemolymph

To evaluate the rheological properties of hemolymph filaments, we used the setup shown in Figure 1B. The wound can be probed for only a few minutes after an incision. That is, the time for experimental preparation was long, and when we applied the probe, no dripping occurred. Thus, the wound was partially sealed by the primary clot. Upon placing the probe on the

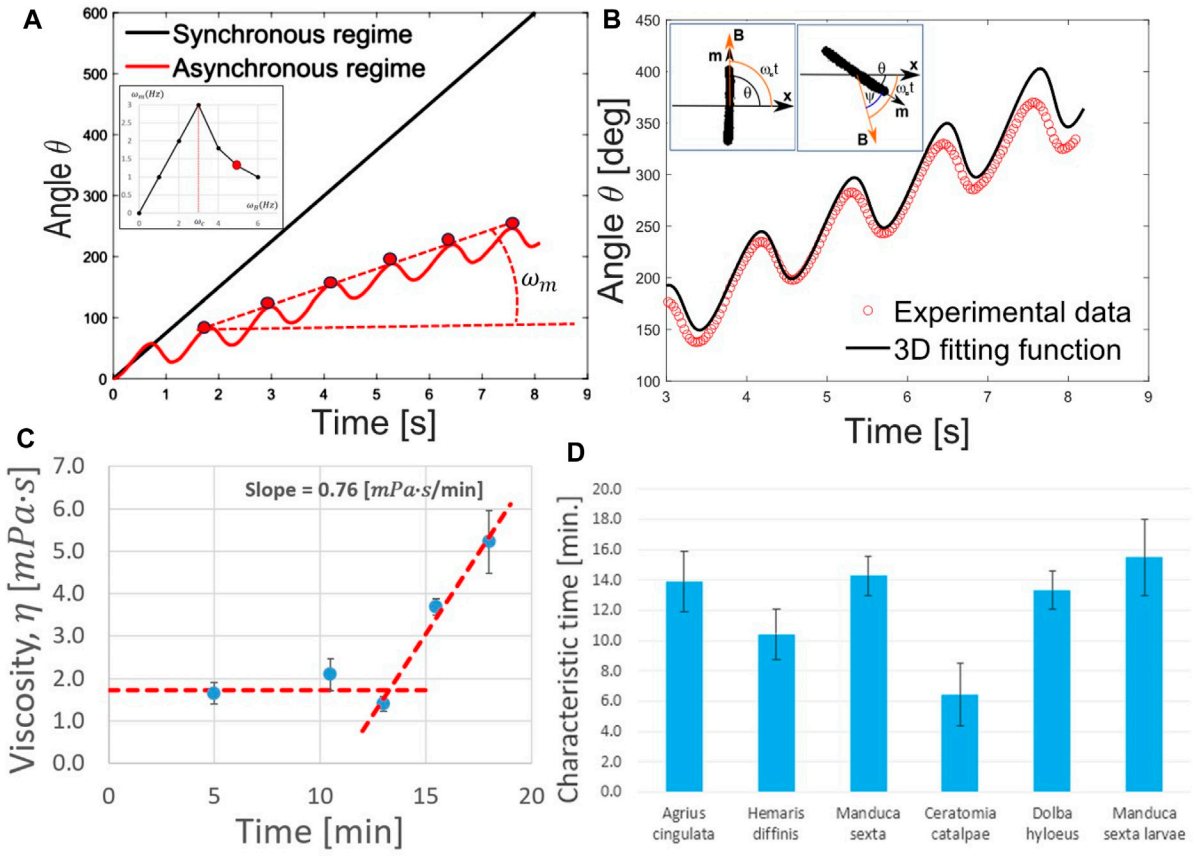


FIGURE 6
**(A)** Angular dependence of $\theta(t)$ on time for the synchronous (black) and asynchronous (red) rotation of the nanorod. The slope of the dashed line provides the average rate of nanorod revolution $\omega_m$ in the asynchronous regime of rotation. The inset illustrates the characteristic master curve used in magnetic rotational spectroscopy. The rate $\omega_m$ of rotation of the nanorod is measured as a function of the frequency of the rotating field $\omega_B$. When the driving frequency is small, $\omega_B < \omega_c$, the nanorod rotates synchronously with the field, $\omega_m = \omega_B$. When the driving frequency reaches a critical frequency $\omega_B = \omega_c$ and increases further, the nanorod rotation changes to asynchronous mode. The descending curve illustrates the effect of enhanced energy dissipation during the asynchronous rotation of the nanorod. The peak value $\omega_c$ is easy to detect in experiments. The red dot in the inset corresponds to this slope of the dashed line. **(B)** In experiments, the magnetic moment ***m*** of a nanorod is always directed along the nanorod axis. Aligning the moment (and hence, the nanorod) parallel to the field ***B***, the reference axis x is set perpendicular to the nanorod axis. Then, rotating the field with frequency $\omega_B$, one tracks the angle $\theta$ that the nanorod axis forms with the x-axis. During nanorod rotation, the angle ψ that the magnetic moment **m** forms with the applied field **B** is not visible. The observed angle θ is then analyzed with the model to evaluate the fluid viscosity. In this example, the experimental data on nanorod rotation in hemolymph were satisfactorily explained by modeling hemolymph as a Newtonian fluid with constant viscosity. **(C)** Viscosity remained constant over minutes. In this example, showing the dependence of the hemolymph viscosity of *M. sexta* larvae, viscosity stayed constant for more than 10 min and then steeply increased. **(D)** Measurements of the time when the viscosity of different lepidopterans (hawkmoths) increased twice the initial value indicated that the shear viscosity remained constant for at least 5 min.

wound and lifting the probe (Figure 1B), we formed the first filament connecting the ball with the wound (Figure 7A). This filament was quite stable; despite the caterpillar's movements, the meniscus that formed at the filament foot slid across the drop surface and did not break (Figures 7B, C). When the wounded proleg was moved up or down, the filament stretched or contracted, respectively (Figures 7E, H). The first filament took 1–20 s to become thin and break up (Figures 7I, J). We call these liquid bridges "long-lived filaments" (LLFs), indicating that their lifetime exceeded 1 s. These long-lived filaments sometimes developed single or multiple droplets, which remained on the filament until its breakup or moved to the ends. The droplet that moved to the wound was re-absorbed by the wound, and the droplet that moved to the ball was re-absorbed by the film on the ball.

When the probe was applied for the second time, the filament was less stable and broke in less than 1 s (Figure 8). We called these filaments "short-lived filaments" (SLFs). They behaved like those dripping from the wound (Figure 3).

After the second trial, when the probe touched the wound and was then raised, the liquid bridges broke in less than 10 ms, following the breakup stages shown in Figure 2. These observations suggested that the hemolymph behaved as a simple low-viscosity Newtonian liquid, like water, that does not form cylindrical filaments (Eggers, 1997; Montanero and Ponce-Torres, 2020) (see an example in Supplementary Video S2).

Using short-lived filaments as representatives of those dripping from the wound and assuming that they would reflect the properties of the dripping filaments, we characterized their rheological properties. The rheological properties of the hemolymph were evaluated by tracking the radius of the short-lived filaments with time. By analyzing the kinetics of liquid-bridge thinning, we discovered that the bridge radius followed the exponential law

TABLE 1 Hemolymph viscosity, body length, body width, and sample size for 19 insect species.

| Common names | Latin names | Hemolymph viscosity, mPa*s | Body length, cm | Body width, cm | Forewing length, cm | Number of individuals | Number of nanorods | Number of measurements |
|---|---|---|---|---|---|---|---|---|
| Lepidoptera species (adults) | Lepidoptera species (adults) | | | | | | | |
| Painted lady butterfly | *Vanessa cardui* | 1.34 ± 0.24 | 2.11 ± 0.08 | 0.50 ± 0.10 | 3.01 ± 0.10 | 14 | 43 | 190 |
| Monarch butterfly | *Danaus plexippus* | 1.44 ± 0.39 | 3.18 ± 0.13 | 0.57 ± 0.11 | 5.16 ± 0.10 | 9 | 16 | 106 |
| Pawpaw sphinx moth | *Dolba hyloeus* | 1.48 ± 0.11 | 3.40 ± 0.14 | 0.96 ± 0.08 | 2.83 ± 0.29 | 5 | 15 | 85 |
| Plebeian sphinx moth | *Paratrea plebeja* | 1.51 ± 0.17 | 3.43 ± 0.35 | 0.99 ± 0.10 | 3.13 ± 0.24 | 5 | 11 | 63 |
| Rustic sphinx moth | *Manduca rustica* | 1.47 ± 0.16 | 5.47 ± 0.27 | 1.55 ± 0.15 | 5.99 ± 0.10 | 5 | 16 | 95 |
| Five-spotted hawkmoth | *Manduca quinquemaculata* | 1.70 ± 0.24 | 5.31 ± 0.44 | 1.23 ± 0.13 | 5.40 ± 0.30 | 7 | 26 | 168 |
| Carolina sphinx moth | *Manduca sexta* | 2.17 ± 0.50 | 4.55 ± 0.49 | 1.10 ± 0.06 | 5.28 ± 0.52 | 19 | 49 | 315 |
| Catalpa sphinx moth | *Ceratomia catalpae* | 2.07 ± 0.33 | 3.40 ± 0.40 | 0.91 ± 0.10 | 4.38 ± 0.48 | 6 | 13 | 72 |
| Pink-spotted hawkmoth | *Agrius cingulata* | 1.85 ± 0.29 | 5.37 ± 0.50 | 1.28 ± 0.07 | 4.80 ± 0.40 | 5 | 21 | 110 |
| Tersa sphinx moth | *Xylophanes tersa* | 1.77 ± 0.29 | 4.01 ± 0.21 | 0.85 ± 0.06 | 3.40 ± 0.20 | 4 | 18 | 99 |
| Pandora sphinx moth | *Eumorpha pandorus* | 1.61 ± 0.14 | 4.86 ± 0.28 | 1.10 ± 0.09 | 4.60 ± 0.50 | 5 | 19 | 123 |
| White-lined sphinx moth | *Hyles lineata* | 1.55 ± 0.28 | 3.87 ± 0.66 | 1.02 ± 0.17 | 3.10 ± 0.20 | 6 | 31 | 174 |
| Snowberry clearwing moth | *Hemaris diffinis* | 1.81 ± 0.12 | 2.72 ± 0.30 | 1.04 ± 0.18 | 2.95 ± 0.06 | 5 | 19 | 104 |
| Mournful sphinx moth | *Enyo lugubris* | 1.83 ± 0.22 | 3.45 ± 0.19 | 0.96 ± 0.11 | 3.67 ± 0.10 | 5 | 18 | 103 |
| Nessus sphinx moth | *Amphion floridensis* | 1.87 I 0.22 | 2.4 ± 0.1 | 0.5 ± 0.1 | 2.3 ± 0.1 | 2 | 6 | 26 |
| Laurel sphinx moth | *Sphinx kalmiae* | 1.43 ± 0.29 | 4.0 ± 0.1 | 0.8 ± 0.1 | 0.9 ± 0.1 | 2 | 4 | 21 |
| Banded sphinx moth | *Eumorpha fasciatus* | 1.36 ± 0.14 | 3.85 ± .50 | 0.82 ± 0.1 | 4.3 ± 0.1 | 3 | 8 | 41 |
| **Lepidoptera species (larvae)** | **Lepidoptera species (larvae)** | | | | | | | |
| Tobacco hornworm | *Manduca sexta* | 1.66 ± 0.37 | 7.8 ± 0.3 | 1.3 ± 0.1 | — | 6 | 11 | 63 |
| **Blattodea species** | **Blattodea species** | | | | | | | |
| American cockroach | *Periplaneta americana* | 1.83 ± 0.41 | 3.5 ± 0.7 | 1 ± 0.2 | 2.7 ± 0.3 | 9 | 27 | 135 |

$$R = R_0 \exp\left(\frac{-t}{3\theta}\right), \quad (1)$$

with relaxation time $\theta$. These kinetics are typically expected for a viscoelastic fluid following the Oldroyd-B constitutive equation (Bazilevsky et al., 1990; Bazilevskii et al., 2001; McKinley and Sridhar, 2002; Rodd et al., 2005; Kojic et al., 2006; Bazilevsky et al., 2011). The Oldroyd-B fluid is characterized by two constants: its shear viscosity $\eta$ and relaxation time $\theta$. The measured relaxation time of this viscoelastic hemolymph ranges between 2 and 4 ms (Figure 9). Figure 3 shows that this estimate of the relaxation time is reasonable. Specifically, three filaments were filmed after the drop fell to the substrate, and the filaments thinned in the same manner as that shown in Figure 8 due to capillary action. The analysis of those filaments yielded an average relaxation time of $\theta \sim 5\,ms$. Thus, filament stabilization in the dripping hemolymph can be explained by its viscoelasticity (Larson, 1999; Bazilevskii et al., 2005).

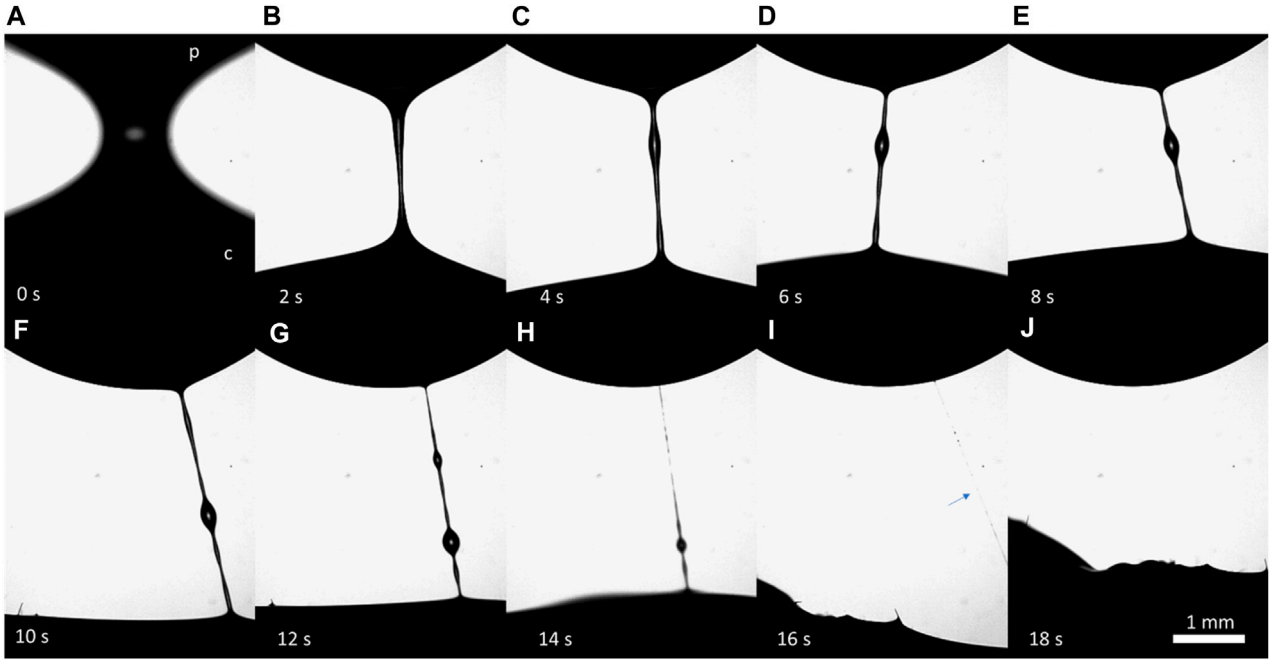


FIGURE 7
**(A–J)** Series of frames illustrating the features of the formation and breakup of a long-lived filament (LLF). The filament formed between a stainless-steel probe (p) at the top and a wound of the *M. sexta* caterpillar (c) at the bottom. The camera was focused on the filament, and the wound was not visible. The caterpillar constantly moved, causing the filament to move.

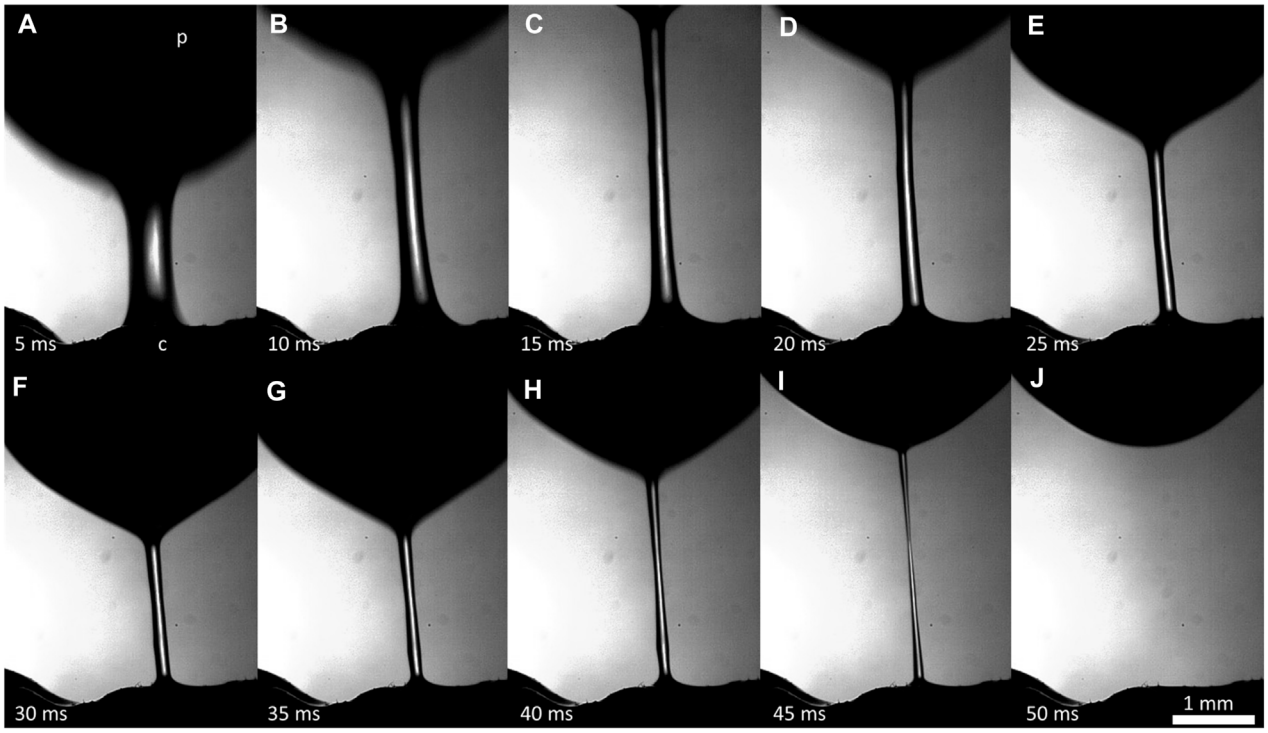


FIGURE 8
**(A–J)** Series of frames illustrating the features of the formation and breakup of a short-lived filament (SLF); (p) is a stainless-steel probe, and (c) is the wound of the *M. sexta* caterpillar. It takes approximately 45 ms for the SLF to break up and disappear.

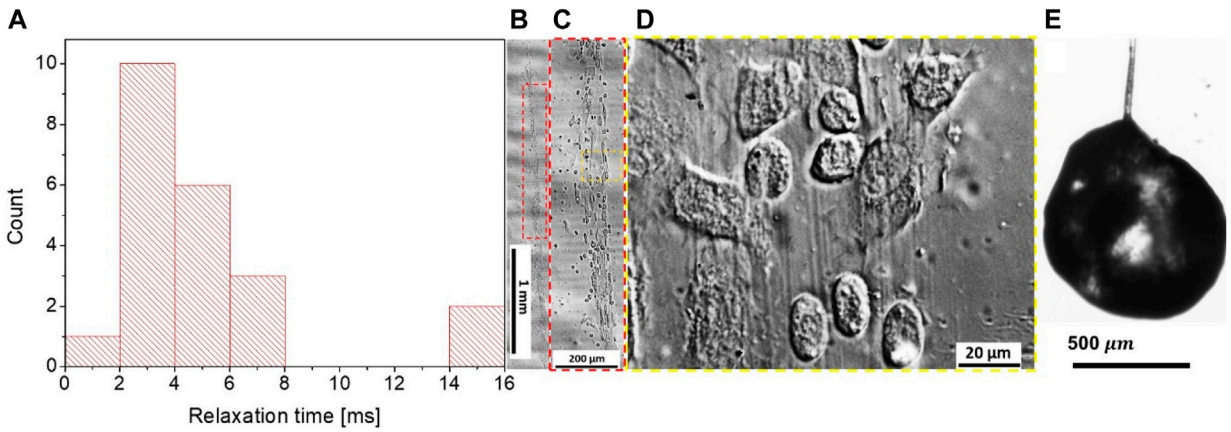


FIGURE 9
**(A)** Relaxation time θ measured for four *M. sexta* caterpillars with 22 liquid bridges. The short-lived filaments appeared to be viscoelastic, and the majority had a relaxation time θ of between 2 and 4 ms. **(B–D)** Phase-contrast optical microscopy of the filamentous core in long-lived filaments. The boxed region in **(B)** is magnified in **(C),** and the box in **(C)** is magnified in **(D)**. The core of the long-lived filament consisted of a network of micron- and submicron-diameter filaments with embedded hemocytes. **(E)** The hanging drop remained on a long-lived filament after forming this filament from the pool of hemolymph, as shown in Figure 1C. The lower filament connecting the drop with the hemolymph pool was naturally broken following the scenario shown in Figure 8, but the weight of the remaining liquid drop was balanced by the stress on the supporting filament. Water naturally evaporated from the filament, while the surface of the drop formed a crust that contained the interior as the liquid hemolymph.

To evaluate the cause of the distinct kinetics of the SLF and LLF thinning, we turned to the structural analysis of their composition. When we probed the wound with the ball in the first 3 min, long-lived filaments were formed 13 times, short-lived filaments were formed 18 times, and 22 trials produced no filaments. For wounds older than 8 min, we observed a long-lived filament only once, while short-lived filaments were observed 11 times, and 52 trials produced no filaments. The long-lived filaments did not necessarily follow the Oldroyd-B model or have a broad dispersion of the relaxation times ranging from milliseconds to seconds. This scattering of the material parameters led us to hypothesize that because of the caterpillar's movements, the ball might have probed the hemolymph from different depths of ball immersion. We suspected that the ball forming the long-lived filaments might have probed the primary clot together with the layer of hemocytes covering the wound surface. Sometimes, the flowing hemocytes can be observed inside the LLF (Supplementary Video S4).

By collecting long-lived filaments on a glass slide and studying them using phase-contrast microscopy, we discovered filamentous cores made up of polymeric filaments with embedded hemocytes (Figures 9B–D). These filaments were long and bundled, even without hemocytes. When a long-lived filament was broken at one end, some droplets sometimes remained on a dried filament and formed a crusted surface, while the interior of the drop remained full of liquid hemolymph (Figure 9E).

These observations confirm that LLFs contain primary clots, and hence, their thinning kinetics is controlled by the deformation and flow of the highly inhomogeneous composite structure of primary clots. The more mature the primary clot is, the slimier it is, and the slower the filament breaks up.

## 2.4 Clotting starts with the interfaces

To further investigate the phenomenon of crust formation, we examined the behavior of hemolymph drops using X-ray micro-CT and SEM imaging. X-ray imaging is attractive because it distinguishes between the structure of the multiphase and multicomponent materials (Andrews et al., 2011; Maire and Withers, 2014). Before submitting the hemolymph drop for X-ray imaging, we rapidly froze the drop on a metal substrate and slowly sublimated the water (as explained in *Materials and methods*). Then, a freeze-dried drop was imaged using an X-ray microscope (Bruker SkyScan 1176). The images were reconstructed (Figures 10A, B), and we schematically show how the cross-sections parallel and perpendicular to the substrate were taken (Figure 10C). These images show the density distribution of primary aggregates or clots through the drop thickness. The material closer to the air/hemolymph and hemolymph/substrate interfaces had a greater density.

To evaluate the microstructure of this interfacial layer, the frozen drop was broken and removed from the substrate. The remaining material that adhered to the substrate was examined by scanning electron microscopy. Figures 10D–F show residues on the substrate from the droplet sitting on it for longer than 20 min before freezing. Chain-like aggregates are observed attached to the substrate. These aggregates are much larger than the individual hemocytes, suggesting that the hemocytes were already assembled into chain-like primary clots. The possible building blocks of these chain-like aggregates are shown in Figure 10E, where solitary aggregates of approximately $30\mu m$ in diameter were found. Filamentary residues covered the boundaries of larger primary clots (Figure 10F). These filaments were like those described by Geng and Dunn (1988) and Geng (1990). No visible filaments were found in the droplets incubated for less than 20 min.

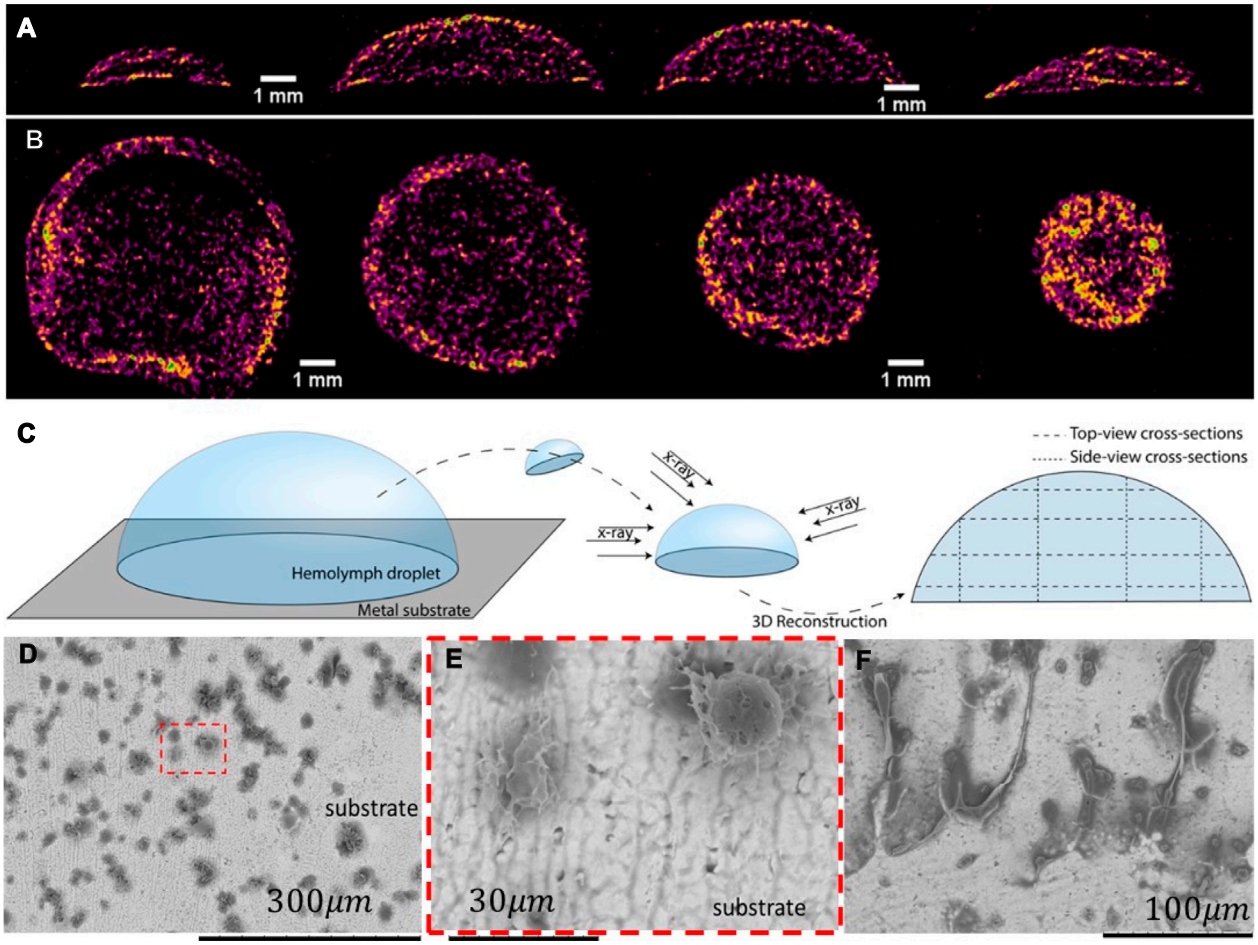


FIGURE 10
Micro-CT scans of a freeze-dried hemolymph drop. Yellow represents a high-density material, and purple represents a low-density material. **(A)** Series of drop cross-sections was taken perpendicular to the substrate, as specified in **(C)**. The cross-sectional area increased from the drop edge to the center. **(B)** Series of drop cross-sections was taken parallel to the substrate, as specified in **(C)**. The cross-sectional area decreased from the substrate to the droplet top. The interfacial layer of the hemolymph appears to have a high-density material. **(C)** Diagram depicting the sample preparation procedure and the locations of the four parallel and perpendicular sections. **(D)** SEM micrographs of hemolymph residues attached to the substrate. Small dark spots form either chain-like or solitary aggregates. **(E)** Solitary aggregates appeared in the framed area in **(D)**. **(F)** Filamentary residues sticking out from the aggregate are also common for larger aggregates.

All these findings favor the hypothesis that in larval Lepidoptera, the primary clots first nucleate at the interfaces and form a crust-like shell preventing water evaporation. The shell propagates inward to occupy the entire drop.

## 2.5 Interfacial interactions between hemocytes in the hemocyte-rich hemolymph

Hemocytes interact with one another closer to the surface. It has long been hypothesized that some hemocytes extrude thread-like projections (i.e., pseudopodia) in response to foreign surfaces; then, other hemocytes adhere to the formed network (Salt, 1970; Gregoire and Rockstein, 1974). This hypothesis implicitly assumes that the hemocyte density is high enough to allow the connection of two neighboring hemocytes by pseudopodia (Wigglesworth, 1937; Salt, 1970).

We investigated this hypothesis by observing the hemocyte behavior in the droplets released from the wound. Within approximately 3 min from the moment of drop formation, the hemocytes from the larvae of *M. sexta* began adhering to each other. When a magnetic nanorod was introduced to the drop, the pseudopodia anchored the nanorods to the hemocyte aggregates (Figure 5F); the nanorods never broke the hemocytes. In contrast to the free nanorods, the nanorods attached to hemocyte aggregates did not make full revolutions (Aprelev et al., 2019). Instead, they beat in response to the applied rotating field around an equilibrium direction, revealing hidden interconnections between hemocytes (Supplementary Video S3). During these oscillations, the surrounding cells moved in unison with the nanorod. Thus, the hemocytes with the attached nanorods mechanically communicated with the neighboring hemocytes that were not visibly connected to one another. A hidden biopolymer network provides a far-field reaction to a local perturbation, engaging hemocytes in the movement. This local perturbation of an oscillating nanorod

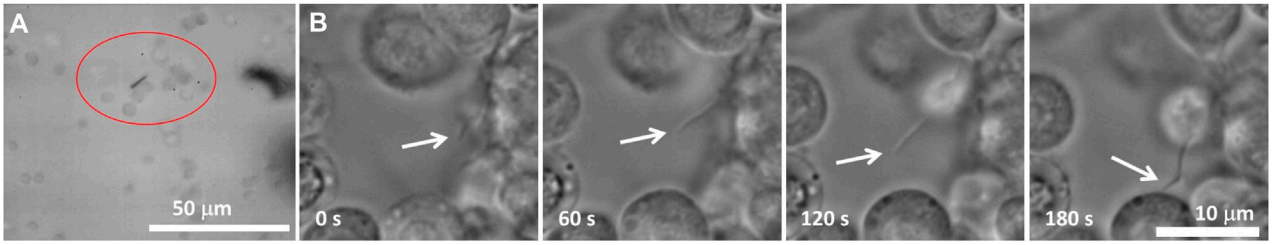


FIGURE 11
**(A)** Image of a nanorod surrounded by a network of cells. The encircled hemocytes are engaged in the movement of the nanorod. As the nanorod attempts to rotate, the hemocytes inside a circled aggregate move together. The hemocytes outside the circle do not respond to the motion of the nanoprobe, indicating that the hemocytes form an aggregate shielding a foreign object from the surrounding hemocytes. **(B)** Phase-contrast image of a growing pseudopodium (arrows). After ~180 s, the two hemocytes become connected through a pseudopodial bridge [adapted from Aprelev et al., 2019].

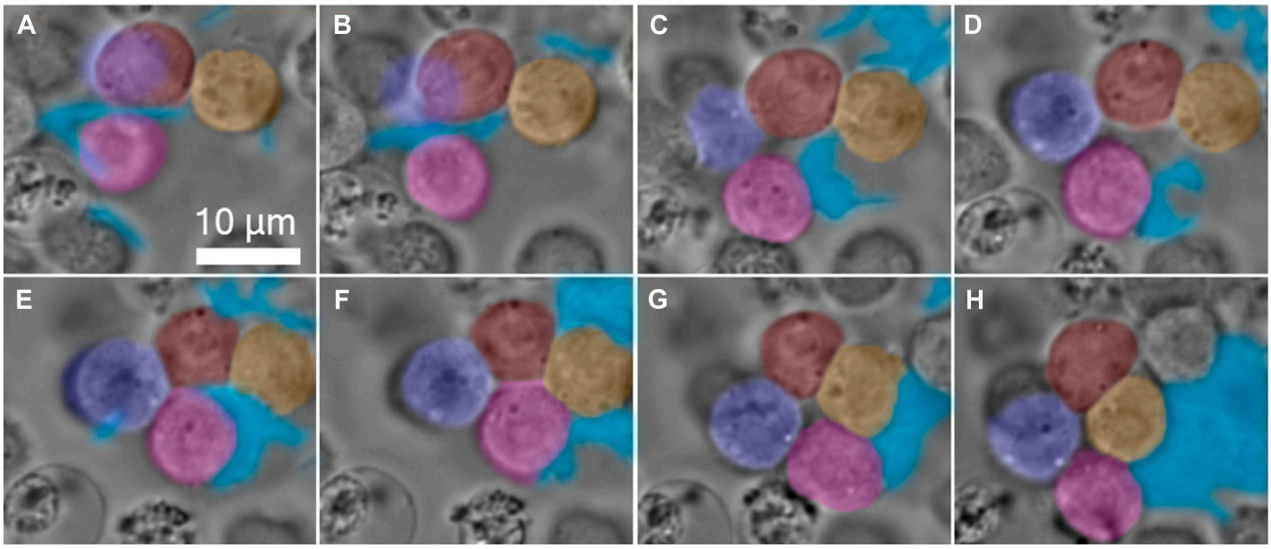


FIGURE 12
Gallery of time-lapse frames, depicting a four-hemocyte aggregate in a primary clot of the hemolymph of a larva of *M. sexta*. The pseudopodia are formed by hemocytes first deforming the interface in finger-like extensions. Each extension could deform and propagate over long distances searching for a target. The hemocytes are artificially colored in red, yellow, purple, and pink, and the aggregate-involved pseudopodia are in blue. **(A)** Initially, the red and yellow hemocytes touch weakly, and the pink hemocyte is free near the extending pseudopodia. **(B,C)** With time, the interface between the red and yellow hemocytes increases, while the pseudopodium attaches to the pink hemocyte and drags it to the right. **(D)** The purple hemocyte, which is attached to both red and pink hemocytes, comes into focus, while the pseudopodium continues to drag the pink hemocyte to the right. **(E)** The red/purple and the pink/purple interfaces grow, and the pink hemocyte, which is half-engulfed in pseudopodia, first touches the red hemocyte. **(F)** The pink hemocyte disconnects from the pseudopodia and attaches to the red and yellow hemocytes. **(G)** The red and pink hemocytes disconnect, and the four-hemocyte aggregate forms a hole in the center. **(H)** The purple and yellow hemocytes form an interface, and the four hemocytes remain in this configuration until the end of the observation [images were extracted from the video in the study by Aprelev et al., 2019].

propagates through an area with a radius of ~5–8 nanorod lengths from the probing nanorod (Figure 11). The analysis of nanorod oscillations in these aggregates suggested that the aggregates with a hidden network that connects them behaved as a viscoelastic material with temporary cross-links (Aprelev et al., 2019), as described by the Green–Tobolsky theory of gels (Green and Tobolsky, 1946).

The high density of hemocytes can only be expected in the neighborhood of the wounded tissue; otherwise, the hemocyte density in a healthy caterpillar is insufficient for hemocyte bridging. We illustrated this statement by showing that after ~3 min of being close to one another in a large population of hemocytes, only two of them were bridged by a pseudopodium; the other hemocytes remained mobile (Figure 11B).

An illustrative scenario of hemocytes gathering in a primary clot during the first 10 min of hemolymph coagulation is presented in Figure 12 (Aprelev et al., 2019). A pseudopodium extends from the originating mother hemocyte, stretches further, and bends on its way, targeting another hemocyte, to which it later adheres. The pseudopodium functions as a hydraulic spring; on its way to finding the target, it stretches the constituent material. After contact, the pseudopodium tends to spread along the hemocyte surface. The tension generated in the hemocyte during stretching tends to relax, squeezing the

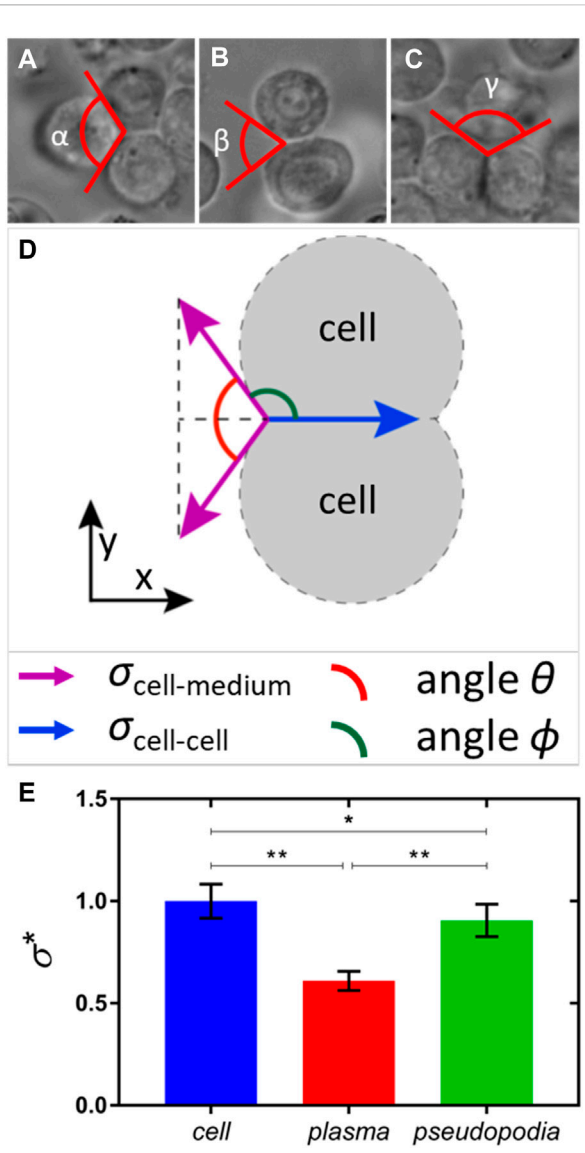


FIGURE 13
Opening angle of the wedge formed by two hemocyte interfaces in different environments. **(A)** When three hemocytes reside in a primary clot and their interfaces form a wedge of angle α filled with the hemocyte interior; **(B)** when two hemocyte interfaces form a wedge of angle β filled with plasma; and **(C)** when two hemocyte interfaces form a wedge of angle γ filled with pseudopodia. **(D)** Free-body diagram for the interfacial tensions acting at the vertex. The associated tensions, the opening angle θ, and the complementary angle ϕ are shown in different colors. **(E)** Bar graph of relative interfacial energies calculated using Eq. 3, where asterisks correspond as follows: *$p$ <0.05 and **$p$ <0.0001. The number of measurements for each scenario is $n_\alpha$ = 12, $n_\beta$ = 14, and $n_\gamma$ = 7.

constituent material back to the mother hemocyte and dragging the targeted hemocyte with it. As the pseudopodium contracts toward the mother hemocyte, it may encounter another hemocyte, attach to it, and bring it to the mother hemocyte. The process repeats, and the aggregates grow larger and change their shape, leading to the formation of a primary clot (Salt, 1970; Gregoire and Rockstein, 1974; Aprelev et al., 2019).

The mechanism of hemocyte adhesion by pseudopodia can be understood from the analysis of the strength of adhesive bonds between hemocytes in the aggregate. The interfacial tensions and the associated interfacial energies of films separating the adjacent hemocytes offer quantitative metrics for the analysis of aggregation phenomena (Figure 13). These interfacial tensions control the opening angle θ, introduced as the angle of the wedge that the two hemocyte interfaces form at contact (Figure 13D). We distinguish the wedges filled with different media of interest. At least three types of wedges could be formed by the two hemocyte interfaces in the primary aggregate when hemocytes contacted each other (Figures 13A–C). When the wedge is filled with the hemocyte interior, and two interfaces in the wedge separate three different hemocytes, the wedge angle is given as θ = α. When the wedge is filled with plasma, and two interfaces separate hemocytes from the plasma, the wedge angle is given as θ = β. When the wedge is filled with pseudopodia, and two interfaces separate hemocytes from the pseudopodia, the wedge angle is given as θ = γ.

We introduce the interfacial tension $\vec{\sigma}_{cell-cell}$ between two identical hemocytes that share a common interface and their interfacial tension $\vec{\sigma}_{cell-medium}$ separating a hemocyte from the surrounding medium (Figure 13D). These vectors are parallel to interfaces and perpendicular to the contact line that runs perpendicular to the figure. In the introduced Cartesian system of coordinates, the $x$-axis is parallel to vector $\vec{\sigma}_{cell-cell}$. Setting up a free-body diagram at the vertex, where three interfaces meet (Figure 13D), we have

$$\vec{\sigma}_{cell-medium} + \vec{\sigma}_{cell-medium} + \vec{\sigma}_{cell-cell} = 0. \quad (2)$$

Balancing the x-components of forces, we obtain

$$\sigma_{cell-medium}\cos\left(\frac{\theta}{2}\right) + \sigma_{cell-medium}\cos\left(\frac{\theta}{2}\right) = \sigma_{cell-cell}. \quad (3)$$

The measured angle α = 120° ± 5° is close to $\alpha$ = 120°, as predicted by Plateau's law (Plateau, 1873) for the bubble and droplet aggregates with the same interfacial tension $\sigma_{cell-cell}$. Therefore, we conclude that these aggregates are formed by the same hemocytes with the same interfacial energy $\sigma_{cell-cell}$. This interfacial energy $\sigma_{cell-cell}$ is assigned for the interfacial energy of hemocytes in the preliminary clot. The relative change in the interfacial energy referenced to $\sigma_{cell-cell}$ is introduced as follows:

$$\sigma^*_{medium} = \sigma_{cell-medium}/\sigma_{cell-cell} = \left[2\cos\left(\frac{\theta}{2}\right)\right]^{-1}. \quad (4)$$

Using the measured angles α = 120° ± 5°, β = 70° ± 11°, and γ = 113° ± 6°, the relative interfacial energies of hemocytes in a primary clot ($\sigma^*_{cell}$), the two-hemocyte aggregate in the plasma ($\sigma^*_{plasma}$), and the two-hemocyte aggregate in pseudopodia ($\sigma^*_{pseudopodia}$) were calculated as $\sigma^*_{cell}$= 1.00 ± 0.08, $\sigma^*_{plasma}$ = 0.61 ± 0.05, and $\sigma^*_{pseudopodia}$ = 0.91 ± 0.08, respectively (Figure 13E). These estimates confirm that pseudopodia form a landing bed for incoming hemocytes, and only ~10% of extra bonds are required to lock the hemocyte in the aggregate.

This analysis emphasizes the importance of interfacial forces in gathering and holding hemocytes together during the development of primary clots.

## 3 Discussion and conclusion

In recent years, the fruitful analogy between the cell aggregates of developing tissues and liquids with a viscoelastic rheology has offered new perspectives in biological soft matter (Steinberg, 2007; Janmey et al., 2009; Gonzalez-Rodriguez et al., 2012; Foty and Steinberg, 2013; Beaune et al., 2014; Beris et al., 2021; Patteson et al., 2022). Although the mainstream research in this direction is focused on vertebrate and human blood, little is known about the material properties of insect blood. We, therefore, investigated the hemolymph clotting phenomena using materials science approaches. The main question that we asked was, "What are the material determinants of fast wound sealing in insects?" By evaluating the rheological properties of the hemolymph over short periods of time, we investigated the mechanisms leading to the arrest of bleeding and to the nucleation and formation of primary clots in insects with hemocyte-rich hemolymph.

Our experiments were triggered by observations of the hemolymph extracted directly from a wound. When a metal pin is dipped in a hemolymph drop with primary clots and then immediately pulled back, one observes a liquid filament bridging the droplet surface using the pin. The hemolymph filament does not break as quickly as a water bridge formed with the same pin drawn from a water droplet. This feature of hemolymph stringing (Gregoire, 1955; Chino et al., 1987; Scherfer et al., 2004; Aprelev et al., 2019) is the first indication of clotting. It can be used for screening different clot inhibitors or promoters, as demonstrated in the hemolymph of fruit fly larvae (*D. melanogaster*) (Bidla et al., 2005; Lesch and Theopold, 2008). Bidla et al. (2005) and Lesch and Theopold (2008) studied the effect of the protein phenoloxidase (PO) on clot tenacity by measuring the maximum pull-out length of the filament in the hemolymph droplets with and without PO. This protein is thought to facilitate the cross-linking and hardening of the primary clot. One would expect that the greater the PO concentration, the harder the clot, and the shorter the pull-out length of the filament before it breaks. This prediction is correct (Bidla et al., 2005; Lesch and Theopold, 2008). Although these observations are useful, no quantitative data on the material properties of the hemolymph have been provided. The most challenging biological question regarding the mechanism of fast wound sealing remain enigmatic.

We found that the larvae of *M. sexta*, which have hemocyte-rich hemolymph, stopped bleeding after 60–90 s. At this time scale, the hemolymph viscosity is low (Table 1), and high-speed videography is needed to film the filament breakup (Figures 2, 3, 8). The appearance of a long cylindrical filament in the dripping hemolymph points to its possible viscoelasticity (Macosko, 1994; Larson, 1999). Many low-shear viscosity biofluids demonstrate viscoelasticity (Bazilevsky et al., 2011; Haward et al., 2011). The hemolymph could behave like saliva dripping from a dog's mouth, with water-level low-shear viscosity, which would still be capable of producing long filaments. Making an aqueous fluid elastic allows an animal to stabilize the flow of blood through the circulatory system or prevent the breakup of liquid bodies, as in the case of dripping hemolymph.

The kinetics of the breakup of a cylindrical filament allows one to evaluate the rheological properties of fluids and distinguish between the specifics of the viscoelastic non-Newtonian behavior of the material (Bazilevsky et al., 1990; Entov and Hinch, 1997; McKinley and Sridhar, 2002). We, therefore, analyzed the kinetics of the filament breakup and observed that before the arrest of bleeding, the hemolymph became viscoelastic with relaxation time $2\,ms$ (Figure 9A).

Knowing the relaxation time and shear viscosity (Table 1), $\eta = 1.66\,mPa \cdot s$, the elastic modulus $G \sim \eta/\theta$ of the elastic additives in the filament can be estimated as $G \sim 2\,Pa$. At least two possible elastic contributors are present in the hemolymph: biopolymers and hemocytes. Collecting the short-lived filaments of interest during bleeding and analyzing them under the microscope, we found no hemocytes. Therefore, the hemolymph elasticity might only come from biopolymers in the hemolymph. Assuming that biopolymers form a weak network, and using the rubber elasticity theory $G \sim \nu k_B T$ (Doi and Edwards, 1988; Larson, 1999), where $k_B$ is the Boltzmann constant and $T$ is the absolute temperature, we can estimate the density $\nu$ of cross-links. At room temperature, $k_B T \approx 10^{-21} J$, the 2-Pa network should contain $\nu \sim 10^{21}\,m^{-3} = 1000 \mu m^{-3}$, that is, a single cross-link is expected per cube with 100-$nm$ sides. Thus, the distance between cross-links is greater than the typical radius of gyration of proteins, suggesting that to self-assemble into bundles, proteins should unfold from their globular state (Erickson, 2009).

Typically, hemolymph plasma contains 0.01–0.1 % w/w of different proteins, some with large molecular weights of up to 500 kDa (He et al., 2016). Geng and Dunn (Geng and Dunn, 1988; Geng, 1990) hypothesized that an insect's immune response causes some fibrous proteins to self-assemble into a network. Among a variety of insect proteins, lipoproteins are known for their ability to self-assemble into chain-like aggregates of more complex biopolymer subunits (Brehelin, 1979; Boman and Hultmark, 1987; Chino et al., 1987; Coodin and Caveney, 1992; Mulnix et al., 1995; Arakawa et al., 1996; Theopold et al., 2004; Rahman et al., 2006; Dushay, 2009; Jiang et al., 2010; Maravilla et al., 2020). Many other fibrous proteins can do the same (Ling et al., 2018; Miserez et al., 2023). Even a minute concentration of chains makes the fluid elastic. For example, even dilute polymer solutions, where polymeric coils are far apart, can stabilize liquid bridges and jets and turn them into constant-radius cylinders (Bazilevskii et al., 2005; Yan et al., 2011; Hoath et al., 2014; Zhang et al., 2022). Therefore, making the hemolymph viscoelastic is critical to stop the bleeding.

Even after the arrest of bleeding, wound closure must be fast to prevent water and solute loss, maintain hydrostatic pressure, and form a barrier against infection. At this step, the viscoelasticity of the low-viscosity hemolymph does not help much, and the insect develops a new strategy by forming a clot that spreads to form a stiff wound seal. The hemocyte-rich hemolymph contains adhesive and non-adhesive hemocytes (Salt, 1970; Lavine and Strand, 2002; Ribeiro and Brehélin, 2006). One scenario of clot nucleation assumes that adhesive cells aggregate at the wound surface or any other surface (Gregoire, 1953; Lai-Fook, 1966; Wigglesworth and Gupta, 1979; Brodland, 2002; Steinberg, 2007; Gonzalez-Rodriguez et al., 2012; Mattix et al., 2014) and are involved in wound healing, phagocytosis (Gregoire, 1955; Salt, 1970; Arnold and Rockstein, 1974; Rowley and Ratcliffe, 1976; Pech and Strand, 1996; Gillespie et al., 1997; Pech and Strand, 2000; Lavine and Strand, 2002; Ribeiro and Brehélin, 2006), and the regrowth of epidermal cells

(Wigglesworth, 1937; Godt and Tepass, 1998; Hayashi and Carthew, 2004; Carthew, 2005; Bulgakova et al., 2012). In this scenario, primary clots are formed at the wound surface or any other foreign surface. We showed that in the larvae of *M. sexta*, primary clots are formed at the interfaces (Figure 10), which propagate from the damaged surface toward the hemolymph interior. This scenario has also been observed for other insects (Gregoire, 1955; Salt, 1970; Wigglesworth and Gupta, 1979; Theopold et al., 2004).

Hemocytes spread over and embed in a fibrous network of primary clots, as shown by the analysis of the core of long-lived filaments (Figure 9). The importance of interfacial forces in gathering and holding hemocytes together during the development of primary clots is shown in Figures 11, 12 and by the theoretical analysis in Section 2.5.

The Ni-nanorod experiments and phase-contrast imaging of these primary clots showed that fibrous connectors are essential for holding hemocytes inside the aggregate and to form connections between the aggregates. We showed that approximately 90% of the adhesion energy between hemocytes comes from the surrounding fibrous bed. To permanently lock the hemocytes in the aggregate, only ~10% of it needs to be added to the adhesion energy. These additional bonds are formed later in clot development during the consolidation of the aggregates (Aprelev et al., 2019).

In summary, we observed that insects with hemocyte-rich hemolymph develop a two-step strategy to form clots. In the first step, the Newtonian plasma of the hemolymph turns into a non-Newtonian viscoelastic fluid, remaining at very-low viscosity. This transformation allows the retraction of the dripping hemolymph to the wound. In the second step, primary clots nucleate and form a crust at the air–hemolymph and hemolymph–substrate interfaces. The clots propagate from the interface toward the droplet center.

Given the adaptive value of viscous-to-viscoelastic fluid conversion, we expect this physical phenomenon to be widespread in insects and other organisms with hemocyte-rich hemolymph. In addition to insects, for example, hemocyte-rich fluids are present in some mollusks (e.g., snails), where they promote wound healing (Machalowski and Jesionowski, 2021). As the hemocyte density changes with age and the infection level in some insects (Stoepler et al., 2013), we also expect the physical behavior of the hemolymph to change. Intriguing experimental subjects include insects that partition hemocyte-rich and hemocyte-poor hemolymph in the same body. The larvae of at least some mosquito species, for instance, are hemocyte-rich at specific body sites, such as the openings into the heart, where they rapidly mobilize to fight infection (League and Hillyer, 2016).

The period from the initiation of the immune cascade reaction to the first microscopically visual detection of a rheological response of the hemolymph remains the unquantified bridge between molecular biology and materials science. Since the last century (Gregoire, 1953), biologists have known that vertebrate red blood cells can initiate an immune cascade reaction in the hemolymph of insects. The material manifestation of viscous-to-viscoelastic conversion of insect hemolymph in a few seconds is attractive for biomedical applications. We hope that our findings will trigger the interest of biochemists and molecular biologists to design fast-working thickeners for vertebrate blood, including human blood.

# 4 Materials and methods

## 4.1 Larval maintenance

The larvae of *M. sexta* were obtained from Carolina Biological Supply (https://www.carolina.com) or were reared in-house on food from Great Lakes Hornworm (https://www.greatlakeshornworm.com/), with some feeding *ad libitum* on hornworm food obtained from Carolina Biological Supply. The deposited eggs were obtained from adults that emerged in a net enclosure (ca. 27°C and relative humidity ca. 65%). Rearing containers were wide-mouthed 1-L glass jars with strips (ca. 3 × 15 cm) of plastic gutter guard (Frost King Model VX620) as a climbing substrate and food support. Larvae were maintained at controlled room temperature (approximately 25°C) and 24 h of artificial light. To provide gas exchange, the jar lids were replaced with aluminum window screens. Food (ca. 10 mL) was added in the first three instars as needed. In later instars, larvae were removed from jars and placed in clean jars with more food added as needed. The number of larvae per jar was reduced as they grew, with 10 or fewer per jar in the last instars. Larvae entering pre-pupation (i.e., those with a more yellowish thorax, no longer eating, and in a wandering phase) were not used as a source of hemolymph.

## 4.2 Hemolymph extraction

The larvae of *M. sexta*, which were 1–2 days before pre-pupation and weighed more than 8.5 g, were used. The caterpillars were washed free of contaminants with DI water and dried using a paper towel. To minimize the movement of larvae, they were placed in specially designed containers (Figure 1) that gripped the larva along the length of the body while exposing the second and third prolegs. Hemolymph was extracted via a 1–2-mm incision made using a razor blade in the third proleg. The hemolymph exiting the wound was collected on a glass slide or probed directly on the body. All experiments were conducted at 20°C–22°C.

## 4.3 Phase-contrast imaging

To investigate the LLF structure, a liquid bridge was created between a hemolymph drop and the metal ball (Figure 1C). A glass slide was placed next to the ball perpendicular to the drop surface so that the slide touched the ball's side. Pulling the ball parallel to the glass slide above the slide edge stretched the liquid bridge and formed a filament. By moving the ball with the filament toward the glass surface, we deposited the filament on the slide. The deposited filament was covered with a cover slip to prevent evaporation during phase-contrast imaging.

To study cell aggregation, drops of blood were placed under an inverted transmitted-light phase-enhanced microscope (Nikon Eclipse Ti; ×40 Oil Objective, S Fluor, NA = 1.30, DIC H/N2; Photometrics CoolSNAP HQ2 camera, 272-ms exposure, time interval = 1 s), and the cell behavior was recorded. Cellular aggregation during the first 10 min of coagulation was observed under high magnification.

### 4.4 X-ray micro-CT and SEM imaging

A drop of hemolymph was rapidly frozen on a metal block in liquid nitrogen, freeze-dried under vacuum, detached from the metal block, mounted on a low-density Styrofoam block, and imaged using X-ray micro-CT (Bruker SkyScan 1176). The image was digitally reconstructed, and the cross-sections were studied. The methodology can be summarized as follows: an X-ray source in tandem with a detector was rotated around the sample, and projection images of the sample were taken. The images were digitally reconstructed into a three-dimensional structure. The cross-sections of the three-dimensional structure could then be visualized. The resolution of the instrument was 9 μm per pixel, which was inadequate to observe the internal structure of the freeze-dried clots but was sufficient to determine the internal distribution of the material density.

### 4.5 Magnetic rotational spectroscopy

Nickel nanorods of diameter $d \sim 200\,nm - 400\,nm$ and length $L_0 \sim 7\,\mu m - 13\,\mu m$, with a remanent magnetization of $M_r = 224$ kA/m (Aprelev et al., 2017), were dispersed in methanol through sonication. A droplet of the nanorod–methanol suspension was placed on a glass slide and allowed to dry at 23 ± 1°C and 50 ± 20% humidity. The hemolymph was placed on the dried nanorod–methanol residue and stirred with a glass rod to disperse the nanorods. The hemolymph droplets were directly exposed to air (21–23°C). To eliminate any effects of the hemolymph–substrate and hemolymph–air interfaces on viscosity, only nanorods inside the drop ($6\,\mu m$ below the air–hemolymph interface and ~ $6\,\mu m$ above the substrate) were used. The nanorod rotation was filmed, and the videos were processed using LabVIEW and MATLAB algorithms, as explained by Brasovs et al. (2023).

### 4.6 Analysis of the filament rheology

The SLF and LLF breakup was filmed using an IDT Technologies MotionPro X3 camera at 200–900 fps with a resolution of 512–640 pixels and a Grasshopper Point Gray camera at 100–140 fps with a resolution of 1,920–1,200 pixels. The time dependence of the filament radius was obtained with a specially developed LabVIEW Vision Development Module that allowed us to extract and analyze the profile of the liquid bridge for each frame of the videos (Sun et al., 2022; Sun et al., 2023). The module used the IMAQ Extract Contour algorithm to provide the filament profile. Then, the radius of the cylindrical neck of the filament was fit by Eq. 1, and the goodness of fit was evaluated as discussed by Sun et al. (2022) and Sun et al. (2023). The procedure was repeated for each filament, and the average relaxation time for the series was reported.

The LLF hemolymph puddles from 10 caterpillars were tested using the setup shown in Figure 1C. The method required approximately 1.0–1.5 min to collect the hemolymph from the bleeding caterpillar and to prepare the experimental setup. Liquid bridges were formed from the same $5\,mm\,x\,5\,mm$ area of the central spot of the puddles.

## Data availability statement

The original contributions presented in the study are included in the article/Supplementary Material; further inquiries can be directed to the corresponding author.

## Ethics statement

Ethical approval was not required for the study involving animals in accordance with the local legislation and institutional requirements because research on insect blood does not require approval.

## Author contributions

PaA: data curation, formal analysis, investigation, methodology, software, validation, visualization, and writing–review and editing. AB: data curation, formal analysis, investigation, software, validation, visualization, and writing–review and editing. TB: visualization and writing–review and editing. CB: investigation, resources, and writing–review and editing. PeA: formal analysis, funding acquisition, investigation, supervision, and writing–review and editing. KK: conceptualization, formal analysis, funding acquisition, investigation, methodology, project administration, resources, writing–original draft, and writing–review and editing.

## Funding

The author(s) declare that financial support was received for the research, authorship, and/or publication of this article. This work was partially supported by the NSF grant IOS 2014664, by the Clemson University Creative Inquiry project to KK, and by the SC BioCRAFT facilities supported by the National Institute of General Medical Sciences (NIGMS) of the National Institutes of Health under award number P30GM131959 through the voucher program to KK. The work of PeA was also partially supported by the NIFA/USDA, under project number SC-1700527, with technical contribution no. 7237 of the Clemson University Experiment Station. The work of PaA was partly supported by NASA through the SC Space Grant Consortium Graduate Assistantship, NASA grant: NNX15AL49H.

## Acknowledgments

The authors thank Guzeliya Korneva and Bryan Wiggers for helping with the optical imaging and characterization of hemolymph properties and Ahva Zadeh for helping them collect the MRS data on the hemolymph of cockroaches.

## Conflict of interest

The authors declare that the research was conducted in the absence of any commercial or financial relationships that could be construed as a potential conflict of interest.

## Publisher's note

All claims expressed in this article are solely those of the authors and do not necessarily represent those of their affiliated organizations, or those of the publisher, the editors, and the reviewers. Any product that may be evaluated in this article, or claim that may be made by its manufacturer, is not guaranteed or endorsed by the publisher.

## Supplementary material

The Supplementary Material for this article can be found online at: https://www.frontiersin.org/articles/10.3389/frsfm.2024.1341129/full#supplementary-material

## References


Andrews, J. C., Meirer, F., Liu, Y. J., Mester, Z., and Pianetta, P. (2011). Transmission X-ray microscopy for full-field nano imaging of biomaterials. *Microsc. Res. Tech.* 74 (7), 671–681. PubMed PMID: WOS:000292570900011. doi:10.1002/jemt.20907

Aprelev, P., Bruce, T. F., Beard, C. E., Adler, P. H., and Kornev, K. G. (2019). Nucleation and formation of a primary clot in insect blood. *Sci. Rep.* 9, 3451. doi:10.1038/s41598-019-40129-0

Aprelev, P., McKinney, B., Walls, C., and Kornev, K. G. (2017). Magnetic stage with environmental control for optical microscopy and high-speed nano- and microrheology. *Phys. Fluids* 29 (7), 072001. PubMed PMID: WOS:000406765200003. doi:10.1063/1.4989548

Arakawa, T., Kato, Y., Hattori, M., and Yamakawa, M. (1996). Lipophorin: a carrier for lipids in insects participates in superoxide production in the haemolymph plasma. *Insect Biochem. Mol. Biol.* 26 (4), 403–409. PubMed PMID: WOS:A1996UQ42100011. doi:10.1016/0965-1748(95)00110-7

Arnold, J. W. (1974). "The hemocytes of insects," in *The physiology of insecta 5* Editor M Rockstein. 2nd ed. (New York: Academic Press), 201–254.

Bazilevskii, A. V., Entov, V. M., and Rozhkov, A. N. (2001). Breakup of an Oldroyd liquid bridge as a method for testing the rheological properties of polymer solutions. *Polym. Sci. Ser. A* 43 (7), 716–726. PubMed PMID: WOS:000170282300008.

Bazilevskii, A. V., Meyer, J. D., and Rozhkov, A. N. (2005). Dynamics and breakup of pulse microjets of polymeric liquids. *Fluid Dyn.* 40 (3), 376–392. PubMed PMID: WOS:000207870400005. doi:10.1007/s10697-005-0078-4

Bazilevsky, A. V., Entov, V. M., and Rozhkov, A. N. (1990). *Liquid filament microrheometer and some of its applications* (Edinburgh, UK: The Golden Jubilee Meeting of the British Society of Rheology and Third European Rheology Conference).

Bazilevsky, A. V., Entov, V. M., and Rozhkov, A. N. (2011). Breakup of a liquid bridge as a method of rheological testing of biological fluids. *Fluid Dyn.* 46 (4), 613–622. PubMed PMID: WOS:000294174000011. doi:10.1134/s0015462811040119

Beaune, G., Stirbat, T. V., Khalifat, N., Cochet-Escartin, O., Garcia, S., Gurchenkov, V. V., et al. (2014). How cells flow in the spreading of cellular aggregates. *Proc. Natl. Acad. Sci. U. S. A.* 111 (22), 8055–8060. PubMed PMID: WOS:000336687900051. doi:10.1073/pnas.1323788111

Beris, A. N., Horner, J. S., Jariwala, S., Armstrong, M. J., and Wagner, N. J. (2021). Recent advances in blood rheology: a review. *Soft Matter* 17 (47), 10591–10613. PubMed PMID: WOS:000719451600001. doi:10.1039/d1sm01212f

Bidla, G., Lindgren, M., Theopold, U., and Dushay, M. S. (2005). Hemolymph coagulation and phenoloxidase in larvae. *Dev. Comp. Immunol.* 29, 669–679. PubMed PMID: 15854679. doi:10.1016/j.dci.2004.11.007

Bohn, H. (1986). "Hemolymph clotting in insects," in *Immunity in invertebrates, cells, molecules and defense reactions*. Editor M. Brehelin (Heidelberg: Springer), 188–207.

Boman, H. G., and Hultmark, D. (1987). Cell-free immunity in insects. *Annu. Rev. Microbiol.* 41, 103–126. PubMed PMID: WOS:A1987K194900005. doi:10.1146/annurev.mi.41.100187.000535

Brasovs, A., Palaoro, A. V., Aprelev, P., Beard, C. E., Adler, P. H., and Kornev, K. G. (2023). Haemolymph viscosity in hawkmoths and its implications for hovering flight. *Proc. R. Soc. B* 290, 20222185. doi:10.1098/rspb.2022.2185

Brehelin, M. (1979). Hemolymph coagulation in *Locusta-migratoria* - evidence for a functional equivalent of fibrinogen. *Comp. Biochem. Physiol. B-Biochem Mol. Biol.* 62 (4), 329–334. PubMed PMID: WOS:A1979GS50300007. doi:10.1016/0305-0491(79)90098-1

Brodland, G. W. (2002). The differential interfacial tension hypothesis (DITH): a comprehensive theory for the self-rearrangement of embryonic cells and tissues. *J. Biomech. Eng-Trans ASME.* 124 (2), 188–197. PubMed PMID: WOS:000175343800006. doi:10.1115/1.1449491

Bulgakova, N. A., Klapholz, B., and Brown, N. H. (2012). Cell adhesion in Drosophila: versatility of cadherin and integrin complexes during development. *Curr. Opin. Cell Biol.* 24 (5), 702–712. PubMed PMID: WOS:000310943300019. doi:10.1016/j.ceb.2012.07.006

Carthew, R. W. (2005). Adhesion proteins and the control of cell shape. *Curr. Opin. Genet. Dev.* 15 (4), 358–363. PubMed PMID: WOS:000231205400002. doi:10.1016/j.gde.2005.06.002

Chapman, R. F. (2013). *The insects: structure and function*. Cambridge, UK: Cambridge University Press.

Chino, H., Hirayama, Y., Kiyomoto, Y., Downer, R. G. H., and Takahashi, K. (1987). Spontaneous aggregation of locust lipophorin during hemolymph collection. *Insect Biochem.* 17 (1), 89–97. PubMed PMID: WOS:A1987E892900013. doi:10.1016/0020-1790(87)90148-x

Coodin, S., and Caveney, S. (1992). Lipophorin inhibits the adhesion of cockroach (*Periplaneta americana*) hemocytes *in vitro*. *J. Insect Physiology* 38 (11), 853–862. PubMed PMID: WOS:A1992JZ89400005. doi:10.1016/0022-1910(92)90096-v

Doi, M., and Edwards, S. F. (1988). *The theory of polymer dynamics*. (Oxford: Clarendon Press), 391.

Dushay, M. S. (2009). Insect hemolymph clotting. *Cell. Mol. Life Sci.* 66, 2643–2650. PubMed PMID: 19418022. doi:10.1007/s00018-009-0036-0

Eggers, J. (1997). Nonlinear dynamics and breakup of free-surface flows. *Rev. Mod. Phys.* 69 (3), 865–930. PubMed PMID: WOS:A1997XL66500009. doi:10.1103/RevModPhys.69.865

Eleftherianos, I., Heryanto, C., Bassal, T., Zhang, W., Tettamanti, G., and Mohamed, A. (2021). Haemocyte-mediated immunity in insects: cells, processes and associated components in the fight against pathogens and parasites. *Immunology* 164 (3), 401–432. PubMed PMID: WOS:000679933500001. doi:10.1111/imm.13390

Entov, V. M., and Hinch, E. J. (1997). Effect of a spectrum of relaxation times on the capillary thinning of a filament of elastic liquid. *J. Newt. Fluid Mech.* 72 (1), 31–53. PubMed PMID: WOS:A1997XP64400002. doi:10.1016/s0377-0257(97)00022-0

Erickson, H. P. (2009). Size and shape of protein molecules at the nanometer level determined by sedimentation, gel filtration, and electron microscopy. *Biol. Proced. Online* 11, 32–51. PubMed PMID: 19495910. doi:10.1007/s12575-009-9008-x

Foty, R. A., and Steinberg, M. S. (2013). Differential adhesion in model systems. *Wires Dev. Biol.* 2 (5), 631–645. PubMed PMID: WOS:000323306600004. doi:10.1002/wdev.104

Geng, C. (1990). *Studies of hemolymph coagulation in Manduca sexta*. Ph.D. dissertation. West Lafayette, IN: Purdue University Proquest Dissertation Publishers.

Geng, C. X., and Dunn, P. E. (1988). Hemostasis in larvae of *Manduca sexta*: formation of a fibrous coagulum by hemolymph proteins. *Biochem. Biophys. Res. Commun.* 155 (2), 1060–1065. PubMed PMID: WOS:A1988Q050400077. doi:10.1016/s0006-291x(88)80604-1

Gillespie, J. P., Kanost, M. R., and Trenczek, T. (1997). Biological mediators of insect immunity. *Annu. Rev. Entomology* 42, 611–643. PubMed PMID: WOS:A1997WD49500025. doi:10.1146/annurev.ento.42.1.611

Godt, D., and Tepass, U. (1998). Drosophila oocyte localization is mediated by differential cadherin-based adhesion. *Nature* 395 (6700), 387–391. PubMed PMID: WOS:000076083800055. doi:10.1038/26493

Gonzalez-Rodriguez, D., Guevorkian, K., Douezan, S., and Brochard-Wyart, F. (2012). Soft matter models of developing tissues and tumors. *Science* 338 (6109), 910–917. PubMed PMID: WOS:000311083600035. doi:10.1126/science.1226418

Green, S. M., and Tobolsky, A. V. (1946). A new approach to the theory of relaxing polymeric media. *J. Chem. Phys.* 14, 80–92. doi:10.1063/1.1724109

Gregoire, C. (1974). "Hemolymph coagulation," in *The physiology of insecta. 5*. Editor M. Rockstein (New York: Academic Press), 309–360.

Gregoire, C. H. (1953). Blood coagulation in Arthropods. HI. Reactions of insect hemolymph to coagulation inhibitors of vertebrate blood. *Biol. Bull.* 104 (3), 372–393. PubMed PMID: BCI:BCI19532700027216. doi:10.2307/1538491

Gregoire, C. H. (1955). Blood coagulation in arthropods. V. Studies on hemolymph coagulation in 420 species of insects. *Arch. Biol.* 66 (1), 103–148. PubMed PMID: BCI: BCI19563000004464.

Gu, Y., and Kornev, K. G. (2016). Ferromagnetic nanorods in applications to control of the in-plane anisotropy of composite films and for *in situ* characterization of the film rheology. *Adv. Funct. Mater.* 26 (22), 3796–3808. PubMed PMID: WOS:000379128700004. doi:10.1002/adfm.201504205

Haward, S. J., Sharma, V., and Odell, J. A. (2011). Extensional opto-rheometry with biofluids and ultra-dilute polymer solutions. *Soft Matter* 7 (21), 9908–9921. PubMed PMID: WOS:000296026700017. doi:10.1039/c1sm05493g

Hayashi, T., and Carthew, R. W. (2004). Surface mechanics mediate pattern formation in the developing retina. *Nature* 431 (7009), 647–652. PubMed PMID: WOS:000224299300030. doi:10.1038/nature02952

He, Y., Cao, X. L., Zhang, S. G., Rogers, J., Hartson, S., and Jiang, H. B. (2016). Changes in the plasma proteome of *Manduca sexta* larvae in relation to the transcriptome variations after an immune challenge: evidence for high molecular weight immune complex formation. *Mol. Cell. Proteomics* 15 (4), 1176–1187. PubMed PMID: WOS:000373992600001. doi:10.1074/mcp.M115.054296

Hillyer, J. F., and Strand, M. R. (2014). Mosquito hemocyte-mediated immune responses. *Curr. Opin. Insect Sci.* 3, 14–21. PubMed PMID: WOS:000209578700004. doi:10.1016/j.cois.2014.07.002

Hoath, S. D., Vadillo, D. C., Harlen, O. G., McIlroy, C., Morrison, N. F., Hsiao, W. K., et al. (2014). Inkjet printing of weakly elastic polymer solutions. *J. Newt. Fluid Mech.* 205, 1–10. PubMed PMID: WOS:000333857000001. doi:10.1016/j.jnnfm.2014.01.002

Hu, H. W., Hu, Q. B., Weng, Q. F., and Wang, J. J. (2024). Hemocytin, the special aggregation factor connecting insect hemolymph immunity, a potential target of insecticidal immunosuppresant. *Pesticide Biochem. Physiology* 198, 105704. PubMed PMID: WOS:001135149200001. doi:10.1016/j.pestbp.2023.105704

Janmey, P. A., Winer, J. P., and Weisel, J. W. (2009). Fibrin gels and their clinical and bioengineering applications. *J. R. Soc. Interface* 6 (30), 1–10. PubMed PMID: WOS:000262756800001. doi:10.1098/rsif.2008.0327

Jeffery, G. B. (1922). The motion of ellipsoidal particles in a viscous fluid. *Proc. R. Soc. Lond. Ser. a-Containing Pap. a Math. Phys. Character* 102 (715), 161–179. PubMed PMID: WOS:000202801300004. doi:10.1098/rspa.1922.0078

Jiang, H., Vilcinskas, A., and Kanost, M. R. (2010). "Immunity in Lepidopteran insects," in *Invertebrate immunity. Advances in experimental medicine and biology. 708*. Editor K. Soderhall (Berlin: Springer-Verlag Berlin), 181–204.

Kenny, M. C., Giarra, M. N., Granata, E., and Socha, J. J. (2018). How temperature influences the viscosity of hornworm hemolymph. *J. Exp. Biol.* 221 (21), jeb186338. PubMed PMID: WOS:000449824800016. doi:10.1242/jeb.186338

Kojic, N., Bico, J., Clasen, C., and McKinley, G. H. (2006). *Ex vivo* rheology of spider silk. *J. Exp. Biol.* 209 (21), 4355–4362. PubMed PMID: WOS:000242132500027. doi:10.1242/jeb.02516

Kornev, K. G., Gu, Y., Aprelev, P., and Tokarev, A. (2016). "Magnetic rotational spectroscopy for probing rheology of nanoliter droplets and thin films," in *Springer book series on characterization tools for nanoscience and nanotechnology. 6.* Editor CSSR Kumar (New York: Springer), 51–83.

Kornev, K. G., Neimark, A. V., and Rozhkov, A. N. (1999). Physical mechanisms of foam flow in porous media. *Rheol. Ser.* 8, 1151–1182. doi:10.1016/s0169-3107(99)80016-1

Lai-Fook, J. (1966). The repair of wounds in the integument of insects. *J. insect physiology* 12, 195–226. doi:10.1016/0022-1910(66)90136-3

Larson, R. G. (1999). *The structure and rheology of complex fluids*. New York: Oxford University Press, 663.

Lavine, M. D., and Strand, M. R. (2002). Insect hemocytes and their role in immunity. *Insect Biochem. Mol. Biol.* 32, 1295–1309. PubMed PMID: 12225920. doi:10.1016/s0965-1748(02)00092-9

League, G. P., and Hillyer, J. F. (2016). Functional integration of the circulatory, immune, and respiratory systems in mosquito larvae: pathogen killing in the hemocyte-rich tracheal tufts. *Bmc Biol.* 14, 78. PubMed PMID: WOS:000383839100001. doi:10.1186/s12915-016-0305-y

Lesch, C., and Theopold, U. (2008). "Methods to study hemolymph clotting in insects," in *Insect Immunology*. Editor N. E. Beckage (Academic Press), 1–12.

Ling, S. J., Kaplan, D. L., and Buehler, M. J. (2018). Nanofibrils in nature and materials engineering. *Nat. Rev. Mater* 3 (4), 18016. PubMed PMID: WOS:000430173500002. doi:10.1038/natrevmats.2018.16

Machalowski, T., and Jesionowski, T. (2021). Hemolymph of molluscan origin: from biochemistry to modern biomaterials science. *Appl. Phys. a-Materials Sci. Process.* 127 (1), 3. PubMed PMID: WOS:000597637300001. doi:10.1007/s00339-020-04166-1

Macosko, C. W. (1994). *Rheology: principles, measurements, and applications*. New York: Wiley VCH.

Maire, E., and Withers, P. J. (2014). Quantitative X-ray tomography. *Int. Mater. Rev.* 59 (1), 1–43. PubMed PMID: WOS:000330498000001. doi:10.1179/1743280413y.0000000023

Maravilla, E., Le, D. P., Tran, J. J., Chiu, M. H., Prenner, E. J., and Weers, P. M. M. (2020). Apolipophorin III interaction with phosphatidylglycerol and lipopolysaccharide: a potential mechanism for antimicrobial activity. *Chem. Phys. Lipids* 229, 104909. PubMed PMID: WOS:000531098600005. doi:10.1016/j.chemphyslip.2020.104909

Mattix, B., Olsen, T. R., Gu, Y., Casco, M., Herbst, A., Simionescu, D. T., et al. (2014). Biological magnetic cellular spheroids as building blocks for tissue engineering. *Acta Biomater.* 10 (2), 623–629. PubMed PMID: WOS:000330921700006. doi:10.1016/j.actbio.2013.10.021

McKinley, G. H., and Sridhar, T. (2002). Filament-stretching rheometry of complex fluids. *Annu. Rev. Fluid Mech.* 34, 375–415. PubMed PMID: WOS:000174038400017. doi:10.1146/annurev.fluid.34.083001.125207

Miserez, A., Yu, J., and Mohammadi, P. (2023). Protein-Based biological materials: molecular design and artificial production. *Chem. Rev.* 123, 2049–2111. PubMed PMID: WOS:000925857700001. doi:10.1021/acs.chemrev.2c00621

Montanero, J. M., and Ponce-Torres, A. (2020). Review on the dynamics of isothermal liquid bridges. *Appl. Mech. Rev.* 72 (1). PubMed PMID: WOS:000525416400003. doi:10.1115/1.4044467

Mulnix, A. B., and Dunn, P. E. (1995). "Molecular biology of immune response," in *Molecular model systems in the Lepidoptera*. Editors M. R. Goldsmith and A. S. Wilkins (Cambridge, UK: Cambridge University Press), 369–396.

Parle, E., Dirks, J. H., and Taylor, D. (2016). Bridging the gap: wound healing in insects restores mechanical strength by targeted cuticle deposition. *J. R. Soc. Interface* 13 (117), 20150984. PubMed PMID: WOS:000378311800003. doi:10.1098/rsif.2015.0984

Patteson, A. E., Asp, M. E., and Janmey, P. A. (2022). Materials science and mechanosensitivity of living matter. *Appl. Phys. Rev.* 9 (1), 011320. PubMed PMID: WOS:000783171000001. doi:10.1063/5.0071648

Pech, L. L., and Strand, M. R. (1996). Granular cells are required for encapsulation of foreign targets by insect haemocytes. *J. Cell Sci.* 109, 2053–2060. PubMed PMID: WOS:A1996VC21500009. doi:10.1242/jcs.109.8.2053

Pech, L. L., and Strand, M. R. (2000). Plasmatocytes from the moth *Pseudoplusia includens* induce apoptosis of granular cells. *J. Insect Physiology* 46 (12), 1565–1573. PubMed PMID: WOS:000090079400007. doi:10.1016/s0022-1910(00)00083-4

Plateau, J. (1873). *Statique Experimentale et The´orique des Liquides Soumis aux Seules Forces Mole´culaires*. Paris: Gauthier-Villars.

Rahman, M. M., Ma, G., Roberts, H. L. S., and Schmidt, O. (2006). Cell-free immune reactions in insects. *J. Insect Physiology* 52 (7), 754–762. PubMed PMID: WOS:000239081500012. doi:10.1016/j.jinsphys.2006.04.003

Ribeiro, C., and Brehélin, M. (2006). Insect haemocytes: what type of cell is that? *J. Insect Physiology* 52, 417–429. PubMed PMID: 16527302. doi:10.1016/j.jinsphys.2006.01.005

Rodd, L. E., Scott, T. P., Cooper-White, J. J., and McKinley, G. H. (2005). Capillary break-up rheometry of low-viscosity elastic fluids. *Appl. Rheol.* 15 (1), 12–27. PubMed PMID: WOS:000233116600004. doi:10.1515/arh-2005-0001

Rowley, A. F., and Ratcliffe, N. A. (1976). The granular cells of *Galleria mellonella* during clotting and phagocytic reactions *in vitro*. *Tissue Cell* 8, 437–446. doi:10.1016/0040-8166(76)90004-5

Salt, G. W. (1970). *The cellular defence reactions of insects*. Cambridge: Cambridge University Press.

Scherfer, C., Karlsson, C., Loseva, O., Bidla, G., Goto, A., Havemann, J., et al. (2004). Isolation and characterization of hemolymph clotting factors in *Drosophila melanogaster* by a pullout method. *Curr. Biol.* 14 (7), 625–629. PubMed PMID: WOS:000220809900030. doi:10.1016/j.cub.2004.03.030

Staczek, S., Zdybicka-Barabas, A., Mak, P., Sowa-Jasilek, A., Kedracka-Krok, S., Jankowska, U., et al. (2018). Studies on localization and protein ligands of *Galleria mellonella* apolipophorin III during immune response against different pathogens. *J. Insect Physiology* 105, 18–27. PubMed PMID: WOS:000427218000003. doi:10.1016/j.jinsphys.2017.12.009

Steinberg, M. S. (2007). Differential adhesion in morphogenesis: a modern view. *Curr. Opin. Genet. Dev.* 17 (4), 281–286. PubMed PMID: WOS:000249366400004. doi:10.1016/j.gde.2007.05.002

Stoepler, T. M., Castillo, J. C., Lill, J. T., and Eleftherianos, I. (2013). Hemocyte density increases with developmental stage in an immune-challenged forest caterpillar. *Plos One* 8 (8), e70978. PubMed PMID: WOS:000324401500055. doi:10.1371/journal.pone.0070978

Strand, M. R. (2008). The insect cellular immune response. *Insect Sci.* 15 (1), 1–14. PubMed PMID: WOS:000252587700001. doi:10.1111/j.1744-7917.2008.00183.x

Sun, Y., Ma, J., Peng, F., and Kornev, K. G. (2022). Making droplets from highly viscous liquids by pushing a wire through a tube. *Phys. Fluids* 34 (3), 032119. doi:10.1063/5.0082003

Sun, Y. M., Bazilevsky, A. V., and Kornev, K. G. (2023). Classification of axisymmetric shapes of droplets on fibers. Could non-wettable fibers support axisymmetric droplets? *Phys. Fluids* 35 (7), 072004. PubMed PMID: WOS:001025235200004. doi:10.1063/5.0151950

Theopold, U., Li, D., Fabbri, M., Scherfer, C., and Schmidt, O. (2002). The coagulation of insect hemolymph. *Cell. Mol. Life Sci.* 59, 363–372. PubMed PMID: 11915949. doi:10.1007/s00018-002-8428-4

Theopold, U., Schmidt, O., Soderhall, K., and Dushay, M. S. (2004). Coagulation in arthropods: defence, wound closure and healing. *Trends Immunol.* 25 (6), 289–294. PubMed PMID: WOS:000222302100004. doi:10.1016/j.it.2004.03.004

Wigglesworth, V. B. (1937). Wound healing in an insect *(Rhodnius prolixus*, Hemiptera). *J. Exp. Biol.* 14 (3), 364–381. PubMed PMID: WOS:000200577900010. doi:10.1242/jeb.14.3.364

Wigglesworth, V. B. (1979). "Hemocytes and growth in insects," in *Insect hemocytes: development, forms, functions, and techniques*. Editor A. P. Gupta (Cambridge, UK: Cambridge University Press), 303–318.

Yan, X. J., Carr, W. W., and Dong, H. M. (2011). Drop-on-demand drop formation of polyethylene oxide solutions. *Phys. Fluids* 23 (10), 107101. PubMed PMID: WOS:000296528000029. doi:10.1063/1.3643269

Zdybicka-Barabas, A., and Cytrynska, M. (2013). Apolipophorins and insects immune response. *Isj-Invertebrate Surviv. J.* 10 (1), 58–68. PubMed PMID: WOS:000328155800001.

Zhang, Z., Peng, F., and Kornev, K. G. (2022). The thickness and structure of dip-coated polymer films in the liquid and solid states. *Micromachines* 13 (7), 982. PubMed PMID:. doi:10.3390/mi13070982